Efficient hydrotreated vegetable oil combustion under partially premixed conditions with heavy exhaust gas recirculation

Fuel 268 (2020) 117350

Contents lists available at ScienceDirect

Fuel

journal homepage: www.elsevier.com/locate/fuel

Full Length Article

Efficient hydrotreated vegetable oil combustion under partially premixed conditions with heavy exhaust gas recirculation

Jacek Hunicz[a,*], Jonas Matijošius[b], Alfredas Rimkus[c], Artūras Kilikevičius[b], Paweł Kordos[a], Maciej Mikulski[d]

[a] Lublin University of Technology, Faculty of Mechanical Engineering, Nadbystrzycka 36, 20-618 Lublin, Poland
[b] Vilnius Gediminas Technical University, Mechanical Science Institute, J. Basanavičiaus 28, LT-03224 Vilnius, Lithuania
[c] Vilnius Gediminas Technical University, Faculty of Transport Engineering, J. Basanavičiaus 28, LT-03224 Vilnius, Lithuania
[d] University of Vaasa, School of Technology and Innovation, Wolffintie 34, FI-65200 Vaasa, Finland

ARTICLE INFO

Keywords:
HVO
Diesel engine
Split injection
EGR
Partially premixed combustion

ABSTRACT

This study performed a detailed analysis of combustion and emission characteristics of a single-cylinder compression ignition engine fuelled with diesel, hydrogenated vegetable oil (HVO) and their blend (50/50). Taking advantage of the high reactivity of HVO, the aim was to investigate how changes in fuel injection and exhaust gas recirculation (EGR) strategies can achieve partially premixed combustion with superior efficiency and ultra-low engine-out emissions. Without EGR, and with a multi-pulse injection strategy optimized for diesel, combustion timings were the same for all three investigated fuels. HVO exhibited higher tolerance to EGR in terms of combustion retarding, so it was possible to use high recirculation rates. This reduced nitrogen oxides, while maintaining high indicated efficiency. The pilot injection control allowed further extending the EGR dilution limit without incurring trade-offs with combustion efficiency and related carbon monoxide and unburned hydrocarbon emissions. Additionally, heavy EGR conditions supported reduction of soot for all three tested fuels. However, the best trade-off between soot and other emission compounds was observed for HVO. HVO also resulted in the lowest emissions of aldehydes and aromatics. In conclusion, on the given engine platform at a steady-state, mid-load operating point, HVO allowed for 43% indicated thermal efficiency with engine-out nitrogen oxides and carbon monoxide emissions near to Euro VI limits. This efficiency level was 1.5 percentage points above that for the optimized diesel operation.

1. Introduction

The last decade has seen a stunning increase in the production of renewable fuels for energy purposes, growing at an average rate of 7.8% per annum. Assuming this trend continues, renewable fuels' share in primary power generation will increase from 4% today to around 15% by 2040 [1]. However, this growth is only enough to cover half of the global increase in energy demand. These numbers indicate that progress towards sustainability is far too slow to meet the greenhouse gas and climate change aspirations of the 2015 Paris Agreement.

In the transport world, although electrification is making progress in the light duty market, diesel engines seem set to remain the prime mover for heavy-duty, long-haul road and marine transport for the coming decades. These sectors are currently responsible for 46% of global transport energy consumption and that proportion is forecast to rise to 50% by 2040 [2]. It is also projected that gasoline consumption will decrease slightly towards 2040 but consumption of diesel fuel (DF) will increase [3]. It is therefore essential that all research effort must not focus purely on developing radical novel propulsion concepts that are still far from commercial implementation. There is an immediate need for parallel work on high technology readiness level (TRL) development (maturing and scaling up) of drop-in, carbon-neutral fuels that can be used in existing compression-ignition engine technology. This development of carbon-neutral fuels needs to be accompanied by intensified combustion research, exploring the full potential of new fuels in terms of efficiency and emission co-optimization. Bearing in mind the urgency of tackling climate change, combustion development should focus on current state-of-the-art technology, harnessing the improvement potential derived from coordinated airpath and combustion control.

Looking at biodiesels, there are currently only two processes that have reached an infrastructural maturity that enables wide-scale

* Corresponding author.
E-mail address: j.hunicz@pollub.pl (J. Hunicz).

https://doi.org/10.1016/j.fuel.2020.117350
Received 19 November 2019; Received in revised form 28 January 2020; Accepted 5 February 2020
Available online 19 February 2020

market implementation. The most commonly used is transesterification of oils using methanol that gives fatty acid methyl esters (FAME). Alternative technology relies on hydroprocessing, which yields hydrotreated vegetable oil (HVO) [4,5]. Although HVO refers to fresh vegetable oils, this type of biodiesel can be produced from a variety of feedstock, including waste biomass such as used cooking oils, animal fats etc. The same applies to FAME, and consequently both fuels can be classified as second generation, not competing with food production [6,7]. It should be noted however, that at their current production scale both HVO and FAME use natural gas to obtain agents necessary for their processes (methanol and hydrogen respectively) and both have similar routes towards full sustainability [8,9]. A comparison of their well-to-wheel CO_2 footprints (i.e. their process energy demand) favours HVO [10].

Even more important for commercial success is fuel quality. HVO is produced by hydrotreating raw feedstock and further isomerisation of the intermediate monoglycerides, diglycerides and carboxylic acids [11], carried out in the presence of a catalyst [12,13]. Depending on individual stages of the process, the resulting products are either pure normal paraffins or mixtures of normal and *iso*-paraffinic hydrocarbons, free from aromatics and sulphur, and with low toxicity [14]. HVO's chemical structure provides good auto-ignition properties and enables clean combustion. FAMEs, on the other hand, are reported to have a propensity to the creation of aldehydes, contributing to toxicity of the exhaust gases [12,15]. Additionally, the polar nature of esters increases their corrosive properties, which is one of the reasons why the EN590 standard limits the proportion of FAME in DF to no more than 7% [16]. Finally, it should be noted that FAME fuels present certain long-term storage challenges whereas this does not apply to HVO [17,18]. In summary, HVO has many advantages compared with FAME.

A fuel's physicochemical parameters affect engine performance and emissions. The mass-based lower heating value (LHV) of HVO is around 2% higher than diesel's but its density is lower. Consequently, HVO's energy density by volume is 5% lower than diesel's [19]. HVO's higher cetane number (CN) gives a faster start of combustion, especially under low and medium engine-loads. With increased in-cylinder temperature, at elevated engine loads, this effect diminishes. The chemical ignition delay, influenced by the CN, becomes then very short and the start of combustion is determined by the time necessary for the fuel spray to form an ignitable mixture with air (physical ignition delay) [20]. Other HVO advantages are shorter primary combustion, better cold-start properties, lower noise and less white smoke [21]. However, due to low lubricity, some authors suggest limiting HVO content to 50% while blending with DF [22].

A more detailed comparison of HVO with mineral diesel shows HVO fuel droplets penetrate through the air stream more easily than diesel's, forming a combustible mixture which is more homogenous. Good mixing results in lower physical ignition delay and better dispersion of the reacting mixture in the combustion chamber, translating into lower local temperatures [23,24]. Vo et al. [22] noted that while using HVO/DF blends not exceeding 30% there is no observable difference in the spray cone angle with respect to the diesel baseline. However, neat HVO's cone angle is significantly wider than diesel's. Similar observations were made by Bohl et al. [23] and Cheng et al. [24]. However, detailed modelling showed that there is virtually no difference in neither liquid fuel penetration nor fuel distribution in the stream. Hulkkonen et al. [25] confirmed this experimentally in an optical engine study. In contrast to the above studies, Preuss et al. [26] investigating HVO spray characteristics in an optically accessible high-pressure injection chamber found that HVO has longer liquid penetration lengths than diesel, whereas the vapour phases exhibit similar penetration. Also, Millo et al. [27] reported a narrower spray cone when only 30% of HVO was admixed to DF. Marasri et al. [28] investigated spray behaviour and combustion of HVO and DF in a high-pressure chamber and under heavy exhaust gas recirculation (EGR) conditions suitable for low temperature combustion. They found that HVO evaporated more easily, and additionally its higher CN significantly reduced auto-ignition delay. It should be noted that both aforementioned properties contribute to auto-ignition timing [29], where in the case of HVO both factors are in favour of auto-ignition advance.

As HVO is commercially available, there are several reports assessing its efficiency and emissions with different types of engines and vehicles. Aatola et al. [4] performed comparative research of emissions and efficiency on a common rail (CR), heavy-duty diesel engine, with split fuel-injection, using DF, HVO and a 30% blend of both fuels. At moderate engine load and speed neat HVO resulted in 30% lower carbon monoxide (CO) and unburnt hydrocarbons (HC) emissions compared with a diesel baseline. There was also a 5% reduction in nitrogen oxides (NO_X) and a 35% reduction in exhaust opacity. Bohl et al. [23] also investigated efficiency and emissions of a CR heavy-duty diesel engine fuelled with DF, HVO and their different blends. Comparing the two neat fuels, their heat release rates were found to be similar at high loads. For low load conditions, however, HVO exhibited earlier combustion of the pilot dose, with roughly the same timing of the main high-temperature combustion phase. Testing over the whole engine-map according to the European Stationary Cycle (ESC) procedure did not show significant differences in emissions of NO_X and particulate matters (PM). Interestingly, emissions of both compounds did not change monotonically with increasing admixture of HVO. Shukla et al. [30], in addition to gaseous exhaust components and PM, investigated the particle number (PN). Heavy duty engine tests, performed under different loads, revealed no significant differences between DF and HVO for any of the mentioned emission quantifiers. Suarez-Bertoa et al. [31] studied DF and its different blends with HVO in a Euro 6-certified passenger car with expanded exhaust aftertreatment system, using the Worldwide Harmonized Light Vehicles Test Cycle (WLTC) emission test. Similarly to previously referred works, the results showed no significant differences in emissions of toxic compounds between DF and HVO, although CO_2 emissions with HVO were 4% lower. However, in this particular case, tailpipe emissions were determined mainly by the performance of particulate filter and NO_X catalytic converter. These results are useful for final conformity validation but the presence of the aftertreatment system means they do not provide insight into differences in combustion or creation of exhaust compounds. Research by Kim et al. [32] on a similar engine, but fitted with only an oxidative reactor, showed that an admixture of 50% HVO resulted in 15% reduction of PM emissions over the NEDC emission test, whereas NO_X emissions increased at higher loads. Interestingly, the same emission results were achieved when HVO was replaced with FAME.

Due to differences in spray formation, some authors suggest regulating injection timing [23] whereas others see no need for injection optimization, especially up to 30% HVO admixture. Aatola et al. [4] used variable engine calibration in terms of start of injection (SoI) timing. The results naturally revealed the well-known NO_X and PM trade-off. For HVO however, the emissions were much smaller than for DF. For example, for the same NO_X calibration, combustion of HVO resulted in 29–42% less smoke. The reverse was also true: calibration for the same smoke level resulted in approximately 30% reduction of NO_X emissions. Advancing and retarding injection by Bohl et al. [23] clearly demonstrated a linear correlation between the SoI and NO_X emissions whereas PN varied according to the quadratic dependence. This research confirmed the previous findings by Aatola et al. [4] indicating that, with split fuel-injections, different auto-ignition properties of HVO and DF affect pilot combustion but the main heat release is nearly the same. Ezzitouni et al. [33] used this fact to justify limiting their HVO optimization strategy solely to pilot injection timings. Their tests using different injection strategies performed for cold starts proved that the potential of paraffinic bio-fuels can be fully exploited only with proper engine calibration.

Some detailed engine studies with HVO also focus on the effects of EGR. Imperato et al. [34], in a large bore engine, explored the potential

of NO_X reduction with HVO and internal EGR, introduced via the miller timing. Over 50% reduction of NO_X emissions was achieved with negative scavenging combined with advanced intake valve closing. This was however occupied by the efficiency penalty due to retarded combustion. Another study by the same group [35] compared HVO and DF in terms of exhaust gas emissions from a single-cylinder heavy-duty engine. The tests simulated EGR by using nitrogen and it was shown that at 30% EGR rate the NO_X reduction was similar for both fuels. However, less exhaust opacity was observed for HVO, making it possible to increase the EGR rate. Vo et al. [22] performed detailed tests of DF and HVO combustion in a rapid compression machine. When using HVO they found the combustion temperature is lower and soot production is reduced. The reduction of O_2 concentration by addition of recirculated combustion products led to a substantial decrease of NO_X for both fuels, but the effect was stronger for HVO. At the same time, PM emission was non-monotonic, peaking at approximately 15% O_2. The drop in PM under heavy EGR conditions was especially noticeable for neat HVO. Millo et al. [27] performed engine tests with single injection, with and without EGR. These revealed different sensitivities for DF and its blend with HVO. In particular, when using the blend (30% HVO, 70% DF), the application of EGR resulted in shorter ignition delay compared to DF. This manifested especially at late fuel injections: the difference diminished towards early injections. Dimitriadis et al. [36] combined the EGR and main injection timing shifts to harness the potential of HVO on a light duty CR engine. It was found that HVO accepts higher EGR rates and later main injection timings providing significant reduction of NO_X emissions, while maintaining lower soot emissions, when compared to DF. The authors of the studies [27] and [36] pointed out the complex response to EGR and injection strategies when using HVO, indicating the need for multi-parameter optimization. Omari et al. [18] investigated engine-out emissions and fuel consumption in the co-optimized scenario. Higher rates of low pressure EGR and reduced fuel-rail pressure were applied to arrive at a dedicated HVO calibration. The results showed that while maintaining NO_X and noise targets similar to the diesel reference, the efficiency of HVO-fuelled engine in a WLTC test increased by 6.3%. That translated into 9% reduction in tank-to-wheels CO_2 emission. More importantly, overall CO, HC and PM emissions were reduced by more than 50%.

Contemporary engine research related to HVO has built on its superior mixing and ignition properties and thus far focused mainly on either optimization of EGR or start of injection (SoI). Many researchers mention the need to co-optimize both parameters but this has not been exploited fully. At the same time, current thinking in diesel combustion is shifting from the “hot” diffusion flame concept towards low temperature combustion. In a single-fuel diesel engine with stock hardware this can be achieved to some extent by realizing partially premixed compression ignition (PPCI), where heavy EGR is applied in combination with multi-injection capability [37]. The resultant faster heat release gives potential for better efficiency, while low temperature combustion curtails NO_X and PM emissions. PPCI technology is on the verge of applicability and some of the latest works on this topic focus on practical implementation of efficient mode-switching strategy [38,39]. However, co-optimization of both efficiency and emissions is limited by the low reactivity of the diesel fuel, which makes it difficult to ignite at high dilution rates [37]. In recent research, Ewphun et al. [40] proposed increasing fuel premixing by means of up to four sequential injections with ultra-high injection pressure. This strategy showed potential to simultaneously increase thermal efficiency and reduce NO_X and smoke but it suffers the limitations associated with spray-wall impingement. Another option is tailoring the fuel reactivity. Singh et al. [39] used diesel blended with ethanol and FAME. These blends do not increase fuel reactivity and hence the results did not satisfy the need for greater efficiency. Pellegrini et al. [41] was among the first to raise the thesis of improving fuel reactivity in striving for PCCI combustion at high EGR rates. HVO and synthetic CN improvers were studied as additives to diesel, using a single-cylinder, light-duty research engine. Despite the limited field of research, this study confirmed that in PCCI mode the fuel CN is the single most influential factor for engine performance.

Summarizing the above literature review, it is evident that the following observations should shape the premise for the present research: (i) in light of the current CO_2 reduction targets, it is necessary to scale-up production of drop-in biofuel (ii) for long-haul transport in particular, HVO combines high TRL level, large feedstock availability and compatibility with other alternatives, with potential for superior efficiency and low emissions in CI combustion engines, especially with dedicated calibration (iii) scaling-up fuel production should be accompanied by corresponding development of high TRL combustion concepts. PPCI is one such concept that builds on HVO’s high CN and low viscosity, while being fully compatible with contemporary combustion engines’ existing hardware (iv) while SoI and the EGR rate are identified as the most relevant parameters for exploiting full engine calibration potential with HVO, the co-calibration of SoI and EGR for low emissions and high efficiency has not been extensively explored (v) despite promising initial results obtained by Pellegrini et al. [41], HVO was not studied for PPCI range extension or efficiency improvement.

Points (i) to (iii) above underpin the justification for the present study: points (iv) and (v) are the two main knowledge gaps that it tackles, using tailored single-cylinder research engine tests. The research, for the first time, explores the boundary of ultra-high EGR rates combined with split injection sweeps, supporting better fuel premixing towards realizing PPCI combustion. The discussion is focused on efficiency and emissions, including both legislated (heavy-duty diesel Euro VI rules) and unlegislated compounds. Insight into the obtained results is provided through in-depth combustion analysis.

2. Materials and methods

2.1. The fuels

Three test fuels are considered in this research: (i) standard, EN590 mineral DF, (ii) neat renewable diesel–HVO with lubricating additives (from Neste [42]) and (iii) 50/50 v/v (HVO50) mixture of DF and HVO. Note that HVO50 is commercially marketed by Neste as “ProDiesel winter” fuel and thus contains additional viscosity improvers. Neither DF nor HVO50 contained any FAME. Table 1 summarises the fuels’ key physical and chemical parameters, along with the determination methods and accuracy. These were characterized in the Water Transport and Environmental Laboratory of Klaipeda University (Lithuania).

Table 1 includes the core properties of HVO that underpin the hypothesis of its suitability for PPCI combustion. Its excellent ignition properties are confirmed by the results of CN analysis, 74.5. The CN for DF is verified as the considerably lower value of 54.1, typical for automotive grade fuels. Similarly, in line with the research premise, HVO’s dynamic viscosity is roughly 10% lower than that of DF, promising better spray atomisation and easier premixing. Note, however, that the kinematic viscosity values of both fuels are similar, due to the difference in their densities.

Looking at HVO50, the effects of improvers is clearly seen because the dynamic viscosity and CN values do not follow the trends dictated by volumetric fractions of both neat fuels. So the flow improver additive greatly reduced HVO50′s viscosity, making it lower than both DF and HVO (at 40 °C the reduction is 33% and 27% respectively). This comes with a trade-off on CN: HVO50′s CN of 59.9 is only slightly higher than the baseline diesel’s 54.1. HVO50′s viscosity/CN trend perturbation allows us to decouple both parameters in the engine tests in terms of their improvement potential towards PPCI. Note that the viscosity improver in HVO50 also reduces the fuel’s oxidative stability. HVO50′s other relevant parameters, however, scale almost linearly between DF and neat HVO.

Table 1
Fuel properties of HVO, DF and their mixture (HVO50).

Properties	Device	Method	Accuracy	Fuel		
				HVO	HVO50	DF
Gross heating value [MJ/kg]	IKA C 5000 calorimeter	DIN 51900-2	130 J/g	47.194	46.685	45.894
Lower heating value (LHV) [MJ/kg]				43.737	43.292	42.825
Cold filter plugging point CFPP [°C]	FPP 5Gs analyser	EN 116	1 °C	−44	−42	−22
Pour point [°C]	CPP 5Gs analyser	ISO 3016	3 °C	−58	−50	−39
Dynamic viscosity at 40 °C [mPa × s]	Anton Paar SVM 3000/G2 Stabinger Viscometer	ASTM D7042	0.1%	2.198	1.611	2.412
Kinematic viscosity at 40 °C [mm^2/s]			0.1%	2.876	2.045	2.940
Density at 40 °C [g/ml]			0.0002 g/cm^3	0.764	0.788	0.820
Dynamic viscosity at 15 °C [mPa × s]				4.014	2.689	4.440
Kinematic viscosity at 15 °C [mm^2/s]				5.136	3.338	5.302
Density at 15°C [g/ml]				0.781	0.805	0.837
Oxidative stability [min]	PetroOXY analyser	EN 16091	0.1%	76.16	70.76	98.0
Water content acc. CF [%]	Aquamax KF Coulometric analyser	ISO 12937	0.0003%	0.0021	0.0022	0.0028
Lubricity [μm/60 °C]	WSD	ISO 12156		344	366	406
Flash point [°C]	FP93 5G2 Pensky-Martens analyser	ISO 2719	0.03 °C	66.3	66.7	70.5
Elemental composition [% wt]	Incineration of samples in a catalytic tube, separation of combustion gases, determination of components by thermal conductivity detector		H	15.3	14.5	13.5
			C	84.7	85.5	86.5
Sulphur [mg/kg]	IKA C 5000 calorimeter, muffle furnace, scales	EN ISO20846		< 1	2.9	6.1
Ash content [% wt]		EN ISO 6245		0.002	0.009	0.014
Cetane number (CN) [-]	PetroSpec analyser	ASTM D613	0.05%	74.5	59.9	54.1

2.2. The engine tests

2.2.1. Experimental set-up and procedures

The study's experimental work was performed at the Lublin University of Technology, Poland. An AVL four-stroke, light-duty single-cylinder CI engine type 5402 CR DI served as the research object. The displaced volume of the test engine was 510 cm^3 and the compression ratio was 17:1. The engine had a toroidal, in-piston combustion chamber with swirl. The cylinder head had a four-valve design with a swirl port (AVL-LEADER concept). The valves were inclined by 3.5°. The fuel was delivered by seven-hole electromagnetic injector and Bosch CP4.1 high-pressure fuel system. A fully open engine-control unit (by Bosch) and Etas INCA software managed the injection parameters. During this research, performed at mid-load regime, the engine was operated as naturally aspirated, so the supercharging system is not discussed here. Exhaust gas was recirculated via a butterfly valve: a cooler provided a constant EGR temperature at the entrance to the intake manifold. An exhaust backpressure valve was installed downstream of the exhaust plenum to enable high EGR rates. Detailed specifications of the test engine are given in Table 2.

Table 2
Research engine specifications.

Type	AVL 5402
Configuration	four-stroke, single-cylinder
Bore	85 mm
Stroke	90 mm
Displacement	510.5 cm^3
Compression ratio	17:1
No. of valves	4
Combustion type	Direct injection
Max. fuel pressure	180 MPa
Injection system	Common Rail CP4.1
Engine management	AVL-RPEMS, ETK7-Bosch
Intake valve opening	712 °CA
Intake valve closing	226 °CA
Exhaust valve opening	488 °CA
Exhaust valve closing	18 °CA
Max. engine load (IMEP)	2.4 MPa

The engine was coupled with an asynchronous motor dynamometer with speed control. The test stand was also equipped with coolant- and lubricant-conditioning systems that guaranteed constant temperature conditions, independent of operating point. The test stand's automation system was based on a programmable logic controller and in-house software.

The fuel delivery system consisted of an AVL 733 S dynamic fuel meter and 753 C fuel temperature conditioner. Additionally, an intake air thermal mass flow meter and low frequency pressure and temperature transducers were installed in the intake runner, exhaust manifold, EGR path, cooling and lubrication systems. Concentrations of gaseous components in exhaust gas were measured with AVL Fourier transform infrared (FTIR) multi-compound analytical system. PM concentrations were measured using a Maha MPM-4 analyser. The excess air ratio (λ) was measured by a LSU 4.2 Bosch lambda probe and an ETAS LA4 lambda meter. Intake O_2 concentration was used to quantify mixture composition at variable EGR ratios. Intake gas was sampled from an intake plenum chamber and analysed using a Hermann-Pierburg HGA 400 gas analyser. The EGR rate was estimated using intake and exhaust CO_2 balance. The detail diagram of the engine test stand is provided in Fig. 1, whereas Table 3 provides the complete list of the measurement equipment, along with respective accuracies.

The combustion analysis was based on in-cylinder pressure measurements. For this purpose, an AVL GU22C pressure transducer was installed directly in the engine head and connected via a charge amplifier to the test bench acquisition system. The high-speed pressure recording was triggered via an optical encoder, with a constant angular resolution of 0.1° crank angle (CA). The acquisition system for the test bench was PC-based with dedicated in-house software.

The mechanical losses of the engine were not considered in the study, so fuel consumption was provided as indicated specific. The directly measured molar concentrations of exhaust gas components were converted to indicated specific emissions, taking into account the indicated specific fuel consumption (ISFC) and the exhaust gas chemical composition. PM emissions were provided by the measurement device in mass per volume units, so exhaust density and fuel consumption were considered to calculate emission factors.

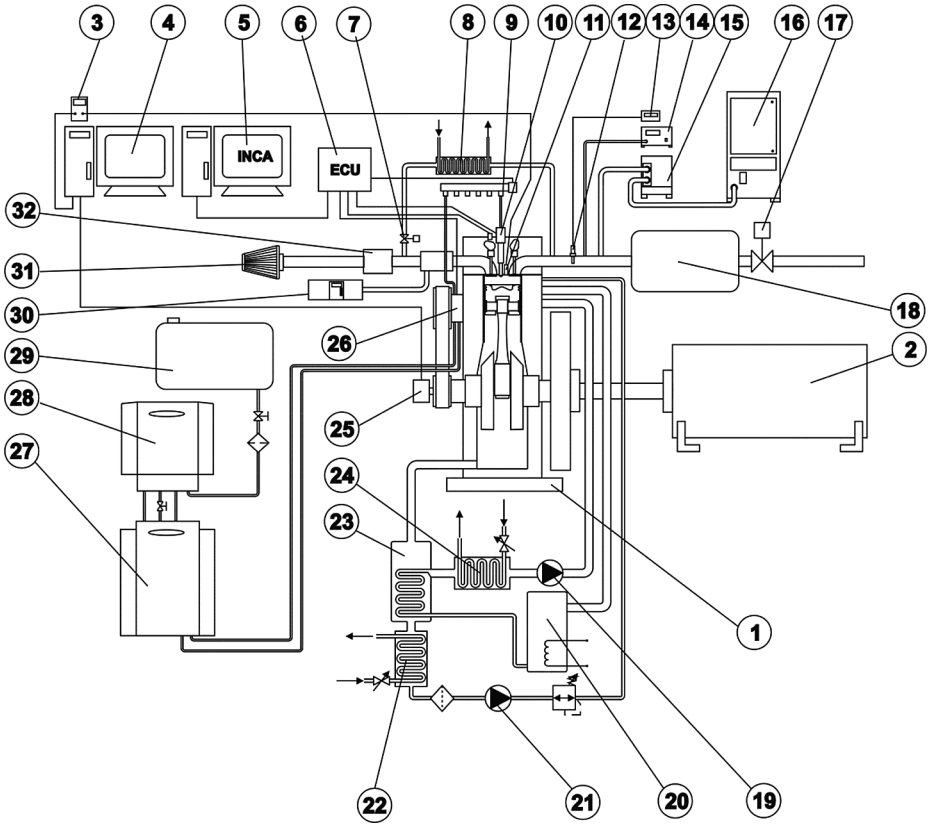

Fig. 1. Diagram of the experimental test stand; 1 – single-cylinder research engine, 2 – AC dynamometer, 3 – charge amplifier, 4 – data acquisition system, 5 – computer with control software, 6 – engine controller, 7 – EGR control valve, 8 – controllable EGR cooler, 9 – fuel rail, 10 – fuel injector, 11 – pressure transducer, 12 – lambda probe, 13 – lambda meter, 14 – MPM-4 soot meter, 15 – heated filter, 16 – FTIR analyser, 17 – exhaust backpressure valve, 18 – exhaust plenum, 19 – coolant pump, 20 – coolant heater, 21 – oil pump, 22 – oil cooler, 23 – oil heater, 24 – coolant cooler, 25 – crankshaft encoder, 26 –high pressure fuel pump, 27 – fuel conditioner, 28 – fuel balance, 29 – fuel tank, 30 – intake gas analyser, 31 – air inlet, 32 – air flow meter.

Table 3
Measurement equipment and accuracy.

Measured quantity	Transducer		Meas. range	Accuracy
In-cylinder pressure	AVL GU22C		0–25 MPa	0.25–1.0%[1)]
Fuel consumption	AVL Fuel Mass Flow Meter 733S		0–125 kg/h	0.12%
Excess air (λ)	Bosch LSU 4.2 / ETAS LA4		0.7–2.8	1.5%
Air mass flow rate	Bosch HFM5		8–370 kg/h	3%
Intake/exhaust press.	WIKA A-10		0–4 bar	0.5%
Temperatures (ambient, intake air, EGR, cooling, oil, fuel)	Pt100 Czaki TP-361		−40–400 °C	0.2%
Exhaust temperature	Thermocouple K Czaki TP-204		0–1200 °C	0.8%
Exhaust composition (gaseous compounds)	AVL Sesam FTIR	CO:HC:NO_X:	1–10000 ppm1–1000 ppm[2)]1–4000 ppm	0.36%0.1–0.49%[3)]0.31%
PM concentration	Maha MPM4		0–700 mg/m^3	0.1 mg/m^3
Intake composition	Hermann-Pierburg HGA 400	CO_2:O_2:	0–20%0–22%	0.1%0.01%

[1)] Depending on temperature.
[2)] Given measurement span relates to concentration of a single identified hydrocarbon.
[3)] Depending on type of hydrocarbon species.

2.2.2. Scope and conditions of the tests

The present experiments focused on exploring a single, mid-load operating point. The rotational speed of the engine was maintained constant at 1500 rpm and the net IMEP for non-EGR operation was around 4.8 bar. The engine was run as naturally aspirated, with ambient intake pressure. Temperatures of the engine coolant and lube oil were set at 85 °C. EGR temperature was maintained at the same level of 85 °C. Fuel rail pressure was 80 MPa and fuel temperature was 30 °C for all experiments.

At each operating point the engine was thermally stabilized (coolant, oil, fuel, EGR) and all governing parameters, except close-loop temperature and rotational speed control, were fixed constant. In-cylinder pressure at each measurement point was acquired for 100 consecutive cycles and then averaged. All slow-changing measurement values, including fuel consumption, were time-averaged by the software for 60 s and then saved.

The experiments were first realized using DF. After completion of the tests with DF all fuel line elements were carefully drained and then, before testing of HVO50, the system was few times flushed with this blend. The same procedure was repeated when switching from HVO50 to HVO.

The experimental matrix consisted of various single and split injection strategies and EGR sweeps. A wide range of EGR rates was enabled by elevated exhaust backpressure (104 kPa absolute). The span of achieved EGR rates versus corresponding intake O_2 concentration is shown in Fig. 2. Note that the relation between O_2 concentration and EGR is not linear due to the presence of excess air in the exhaust. Detail analysis of Fig. 2 shows that there are no significant differences in the stoichiometry between DF, HVO50 and neat HVO. The larger lower heating value (LHV) of HVO is compensated by its higher theoretical air demand. As a result, the LHV of a stoichiometric mixture is nearly the same for all tested fuel samples.

In addition to the straightforward effect on mixture stoichiometry, higher EGR rates increased intake temperature, as evident in Fig. 3.

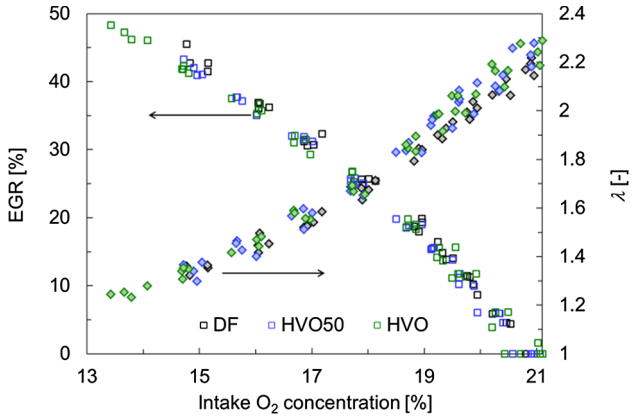

Fig. 2. EGR rate and excess air ratio versus O_2 concentration for all investigated conditions.

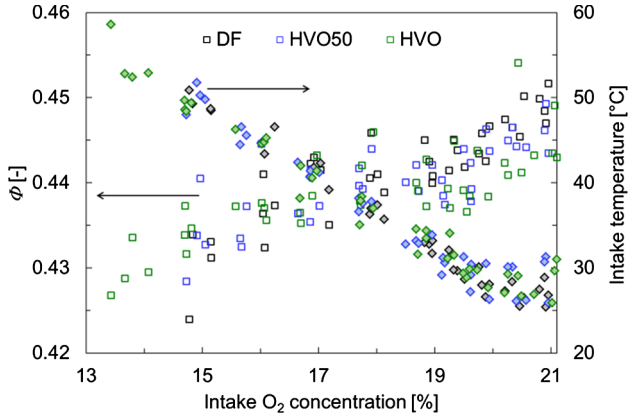

Fig. 3. Equivalence ratio and intake temperature versus O_2 concentration for all investigated conditions.

Note however that the total fuel dilution by exhaust and air was largely insensitive to EGR. In Fig. 3, this is expressed by the equivalence factor (Φ), calculated as a ratio of the air required by stoichiometric proportion and the total air and exhaust on the mass basis.

A split injection strategy was selected as the baseline for this study. The fuel split ratio, with 11% of the total fuel value injected as an early pilot, was established on the basis of a pre-optimization performed without EGR, with lowest NOx/Soot emission as a target. The main injection timing was kept fixed at SoI_2 = 356 °CA. This particular SoI_2 set point was selected to provide controllable combustion onset around TDC, aiming at high indicated efficiency. The explored pilot start of injection (SoI_1) timings were motivated by previous studies on PPCI [43,44]. In search of optimization potential, three SoI_1 timings at 338 °CA, 342 °CA and 346 °CA were applied with the EGR sweps. Previous studies with split injection by Bohl et al. [23] and Ezzitouni et al. [33] showed that recalibration for HVO from the diesel baseline

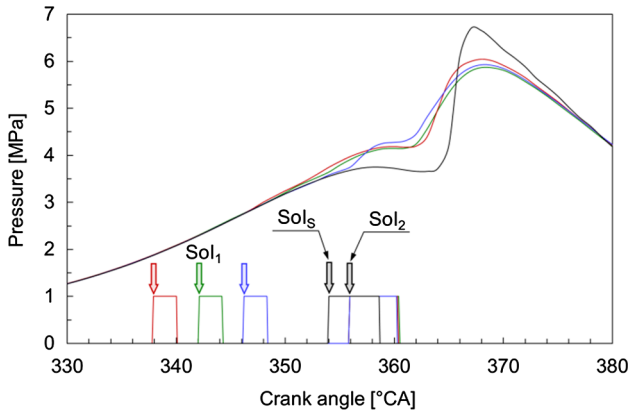

Fig. 4. Injection patterns for HVO50 and corresponding in-cylinder pressures (non-EGR conditions).

can be confined to just varying the pre-injection timing, because fuel ignition quality does not impact the main combustion phase. At the given compression ratio of 17:1 and relatively low intake temperatures, combined with high EGR dilution rates, these injection strategies support PPCI combustion mode, providing the basis for the present study.

Additionally, linking back to earlier HVO studies, conventional diesel combustion (CDC), realized with single injection, was tested at selected EGR conditions. The single injection was commenced at SoI_S = 354 °CA, which without EGR provided the same, performance-optimized CA50 setpoint (365.5 °CA) as for the baseline PPCI configuration (see the Appendix - table A1 for reference). All the other experimental parameters were kept the same as for the split injection baseline.

In order to keep the engine-load constant, the quantity of injected fuel was slightly adjusted during the tests to account for differences in the LHV, density and viscosity of the fuel samples. The adjustment was applied both to pilot injection and the main injection to achieve constant energy input and the same split ratio for all fuels.

The study's complete experimental matrix is presented in Table 4. Graphical presentation of injection strategies and injection durations for HVO50 mixture is provided in Fig. 4, where injection patterns were decoded from the injector coil current. Interestingly, single injection pulse duration is almost the same as second injection for the split injection cases. This is the result of fuel pressure waves after the split injection's pilot injections: pressure drop after pilot injection resulted in reduction of the mass flow rate. For the same reason, the second injection durations differ slightly between SoI_1 timings.

2.2.3. Data analysis.

AVL Boost software was used for detailed heat release rate (HRR) analysis, providing accurate estimations for heat transfer and gas flow. The measured in-cylinder pressure was used as boundary conditions for first-law and gas flow models integrated in the software. The model incorporated the complete EGR path including the valve and the cooler. Cycle-averaged measured values of pressures and temperatures in

Table 4
Scope of the experiments.

Combustion mode	Test protocol	SoI_1 [°CA]	SoI_2 [°CA]	Intake O_2 [%]	EGR rate [%]
Split injection PPCI	Baseline non-EGR	342	356	21	0
	Baseline mid-EGR			16	35
	EGR sweep	338	356	21–14.5[1)]	0–48[1)]
		342			
		346			
Single-pulse CDC	Reference non-EGR	–	354	21	0
	Reference mid-EGR			16	35

[1)] The top boundary in EGR rate was not exploited for DF and blends due to inability to attain stable combustion.

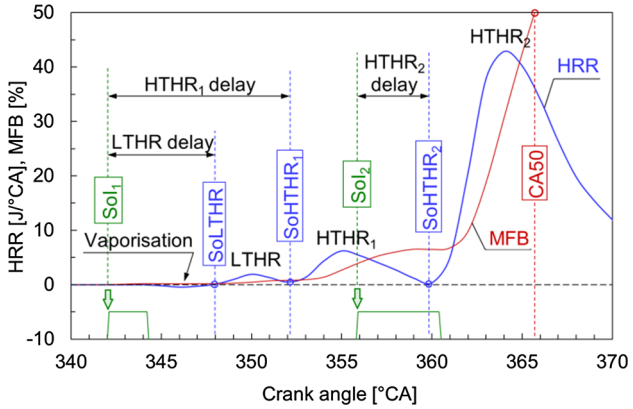

Fig. 5. Example of HRR and MFB curves with their interpretation and definitions of the combustion timing data. Baseline injection strategy (SoI_1 = 342 °CA, SoI_2 = 356 °CA), non-EGR conditions and HVO50 fuel.

intake and exhaust runners were used to calibrate the model.

Detailed calculation flow patterns are not presented, as the approach is standard and commonly used in engine research (see Heywood's Internal combustion engine fundamentals) [45]. It is sufficient to mention that the net HRR was calculated using the first law of thermodynamics, with the ratio of specific heats calculations based on the instantaneous temperature and composition of the in-cylinder mixture. The volume-averaged temperature was calculated using the gas equation of state with consideration of the effect of mixture composition on the gas constant. The Hohenberg model was used to evaluate the heat transfer coefficient and Saint-Venant-Wantzel formula was used to calculate mass flowrates through the valves.

All HRR curves shown in the study refer to the gross values i.e. they include calculated heat transfer rates. The mass fraction burned (MFB) functions were calculated on the basis of cumulative gross heat release. Locations of characteristic points defining combustion advance were read from the HRR and MFB curves and denoted accordingly to Fig. 5. The MFB–derived CA50 (crank angle of 50% mass burned) is used in this work to assess the combustion phasing. Further definitions refer to specific phenomena, recognized for PPCI combustion. These are displayed in Fig. 5 and summarised in the following paragraph.

After the pilot injection at SoI_1 = 342 °CA, the fuel vaporisation phase can be identified, characterized by negative values of HRR. Following that, the low temperature heat release (LTHR) from the pilot dose commences at approximately 348 °CA. The start of LTHR (SoLTHR) is defined as the first CA for which the HRR are > 0. This stage covers low temperature reactions that include both cool flames and negative temperature coefficient region. The start of high temperature heat release from the first fuel dose ($SoHTHR_1$) is visible in Fig. 5, as the local minimum at 352 °CA. The rate of $HTHR_1$ decreases from 355 °CA, due to cumulative effect of reduced reactant concentration from the pilot injection and evaporative cooling of the main injection (SoI_2) at 356 °CA. The next local minimum at around TDC is recognized as the start of the second fuel dose combustion and followed by rapid heat release ($HTHR_2$).

As well as the detailed combustion analysis described above, the combination of experimental measurements and one-dimensional modelling enabled detailed discussion of energy distribution of the individual operating points. Detailed intake and exhaust enthalpy balance with consideration of the EGR loop was used to assess exhaust losses. The heat losses were taken directly from the AVL Boost model described above. Combustion losses are calculated from the chemical balance of total unburned hydrocarbons (THC) and CO. These were multiplied by their LHV to account for energy loss due to incomplete combustion. Note that for simplification, the LHV of DF, HVO50 and neat HVO from Table 1 were used for calculations of THC combustion losses.

3. Results and discussion

3.1. Combustion analysis

3.1.1. Baseline PPCI combustion on different fuels

The combustion of the fuel samples is assessed based on the heat release analysis as discussed in Subsection 2.2.3. Fig. 6 shows pressure, HRR and MFB curves for a non-EGR case and a baseline injection strategy. For all tested fuels, the LTHR starts at the same crank angle of approximately 348 °CA but the burn rates reveal different combustion characteristics. Comparing combustion of DF and HVO, it is evident that HVO exhibits a higher rate of LTHR. While cool flames start approximately at the same time, they are more rapidly followed by the $HTHR_1$ stage of combustion. Interestingly, for HVO50, both combustion phases of the first fuel dose start at the same time as for DF. The amount

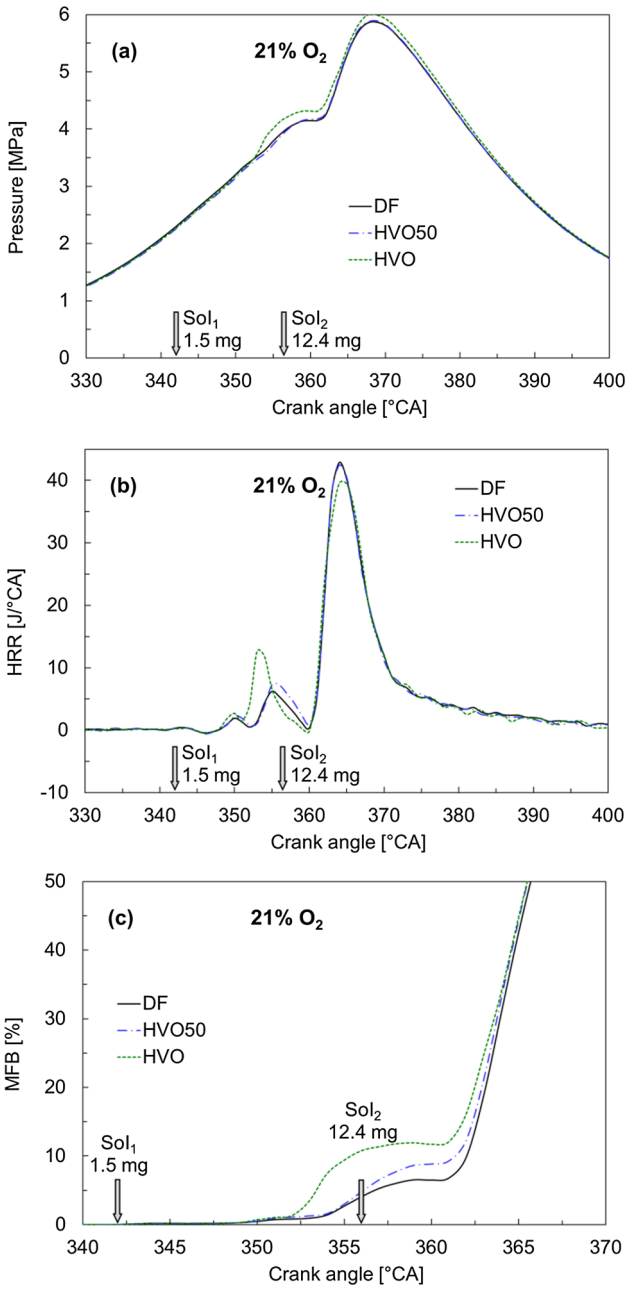

Fig. 6. Pressure (a), heat release rate (b) and percentage of MFB (c) for three investigated fuels at baseline injection strategy (SoI_1 = 342 °CA, SoI_2 = 356 °CA) and non-EGR conditions. Note that x scales differ.

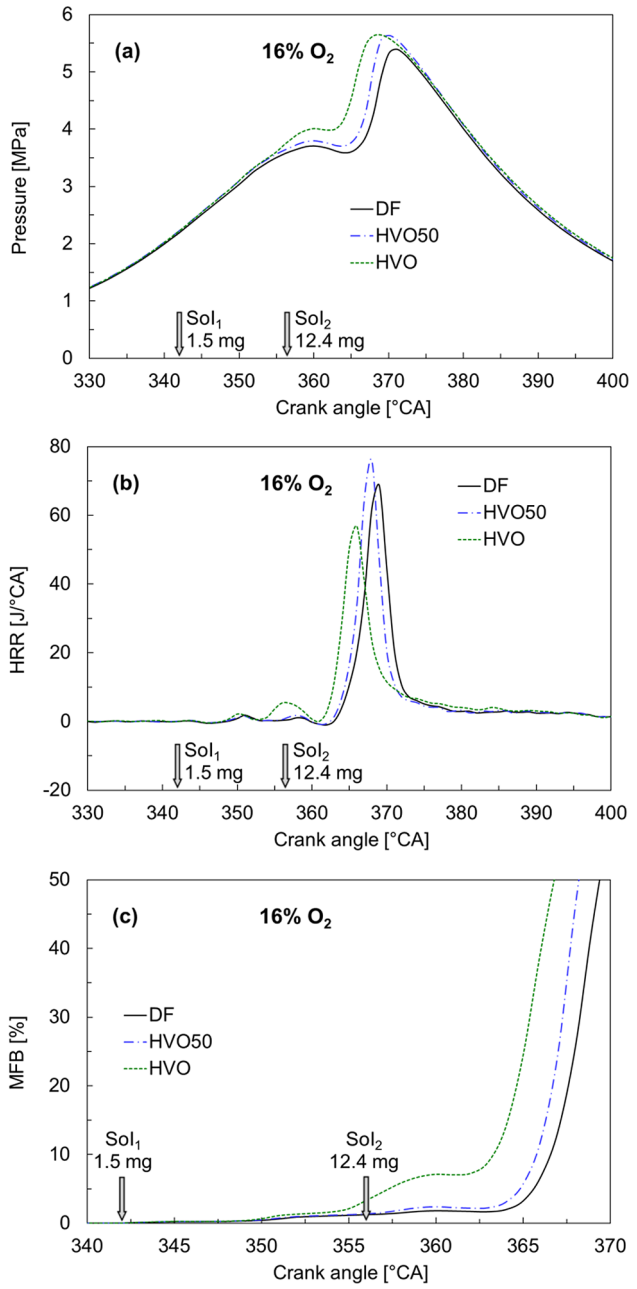

Fig. 7. Pressure (a), heat release rate (b) and percentage of MFB (c) for three investigated fuels at baseline injection strategy (SoI_1 = 342 °CA, SoI_2 = 356 °CA) with EGR providing 16% intake O_2 concentration. Note that x scales differ.

of heat released in $HTHR_2$ stage is, however, slightly higher for the blend. The combustion patterns of early pilot fuel suggest that, for a given condition, the chemical CN effect dominates the physical contribution of mixture preparation, i.e. atomization and evaporation. HVO50's lower viscosity supports better fuel atomization but its diesel-like CN determines start of combustion. Additional insight is provided by Fig. 6c. Comparing MFB curves with the mass of fuel injected, one can immediately note that in the case of HVO, the pilot fuel dose, (approximately 11% fraction of the total fuel quantity) is completely burnt during the $HTHR_1$ period. In contrast, only 55% of the DF pilot is burnt. Detailed analysis of Fig. 6c can help further understanding of the effects of viscosity and CN. As combustion of HVO50 has the same timings as DF, its higher degree of oxidation during the $HTHR_1$ period can be attributed solely to the effect of faster vaporisation.

The $HTHR_2$ period for non-EGR conditions starts at the same time for all tested fuels, resulting in virtually the same CA50 location, as shown in Fig. 6b. This insensitivity suggests that the main combustion is initiated by the hot gases from the HTHR1 stage. With the axisymmetric injector, the long ignition delay of the early-injected pilot causes the hot combustion products of the second stage to be located near the combustion chamber walls. With high injection pressures, the time for the main injection spray front to reach the walls remains largely independent of the viscosity differences between fuel samples. Interestingly, Fig. 6a shows that the peak HRR for HVO is slightly lower than DF's because a greater fuel fraction is already burnt.

The burn rate characteristics for the baseline mid-EGR case, presented in Fig. 7, show that application of EGR makes the differences between the investigated fuels far more evident. For DF and for the HVO50 blend the $HTHR_1$ stage is hardly visible, resulting in significant delay of their $SOHTHR_2$, relative to HVO's. Comparing Fig. 7b with Fig. 6b shows the introduction of EGR causes a drop in HVO's peak LTHR and substantial delay of its $HTHR_1$, but HVO's main fuel combustion timing appears to be largely insensitive to EGR. For HVO the $HTHR_2$ is commenced at 361 °CA, similar to the non-EGR baseline, whereas for DF and HVO50 it is delayed by 1 °CA. It should be noted that longer delay provides more time for mixing. Furthermore, the reduction of the amount of heat released within the early stage increases the amount of chemical energy available in the $HTHR_2$ period. Consequently, combustion is more rapid: the peak HRR in Fig. 7b is almost double that of the non-EGR case. Note, that for the EGR case, the locations of CA50 vary significantly between fuels. For HVO the CA50 is delayed by only 1 °CA when compared to the non-EGR case, but for DF this delay increased to 5 °CA, as shown in Fig. 7c.

In general, combustion characteristics at the given injection strategy indicate that heat release is not limited by spray development. Instead, $HTHR_2$ starts when second injection is almost completed and thus the mixture is already partially premixed in the main combustion phase. The lack of diffusive combustion dominance supports good oxygen entrainment and avoids excessive temperature formation in over-rich spray regions, supporting clean PPCI combustion.

3.1.2. *Effect of EGR on burn rates*

More detailed insight into the response of the tested fuels to EGR is provided by analysing dedicated sweeps for the baseline injection strategy. For brevity, the discussion is narrowed down to HVO and DF. Fig. 8 shows the HRRs for different O_2 concentrations representing selected points of the EGR sweep. Note that for DF, stable combustion is not attainable for EGR rates higher than 42% (15% O_2 concentrations).

Qualitatively, the trends associated with increasing the EGR rate are actually the same for both fuels. Namely, both LTHR and $HTHR_1$ phases are supressed when reducing the oxygen content, which leads to longer ignition delay for the main fuel dose, along with higher peak HRR (cumulative effect with unburned fuel from the 1st and second phases discussed in earlier chapter). Combustion is continually retarded until the limit of stable combustion is reached. This corresponds to peak HRR location shifted beyond approximately 375 CA. For DF, this happens when oxygen content is reduced below 15%; for HVO fuel the dilution limit is at approximately 13% of oxygen. Note, that at the boundary conditions, the main combustion ($HTHR_2$) apparently has two stages. This is due to a very small fraction of fuel burnt during the $HTHR_1$ phase, which is additionally quenched by the vaporisation of the second fuel dose. As a result, the earlier-prepared mixture burns quickly at the beginning of the $HTHR_2$ phase, while the main fuel dose combustion starts with significant delay. Both sub-phases of $HTHR_2$ appear to be premixed in nature in those conditions, yet progress significantly slower than cases with higher oxygen content. The reduced reactions rates are attributed to the expansion process, thermally limiting the kinetic mechanism, at retarded combustion onsets.

The complete combustion timing characteristics for all tested fuels are provided in Fig. 9. This figure confirms the general observation,

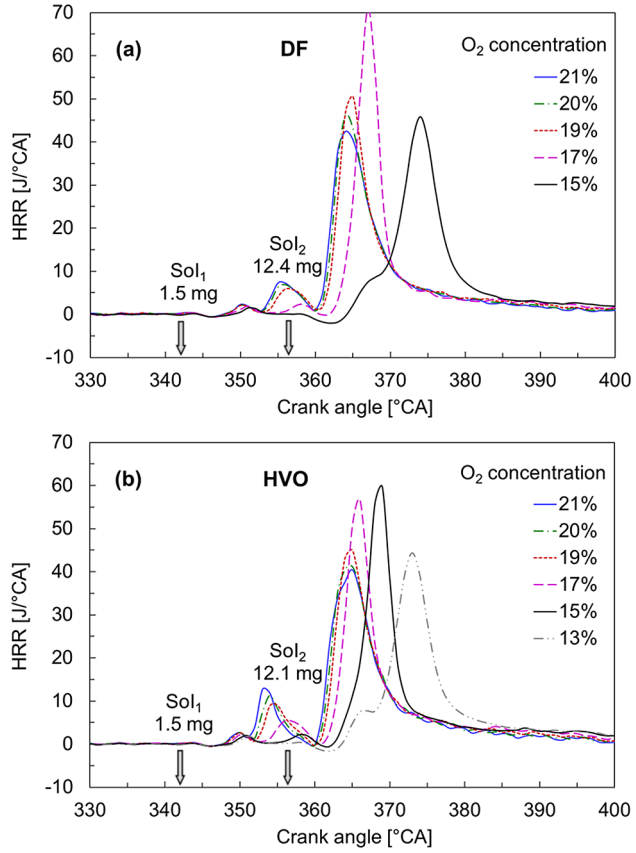

Fig. 8. Heat release rates for variable O_2 concentration at baseline injection strategy (SoI_1 = 342 °CA, SoI_2 = 356 °CA); a) DF, b) HVO.

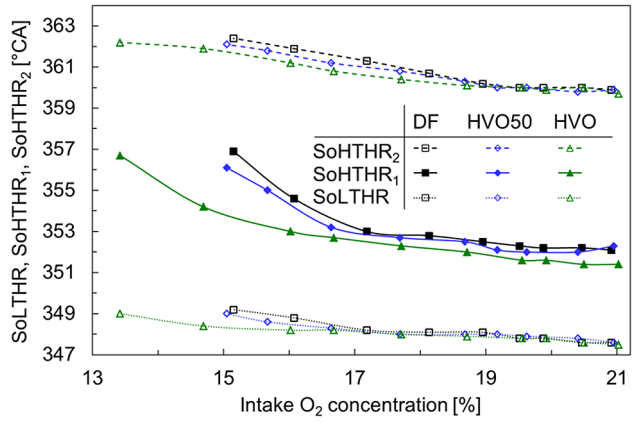

Fig. 9. Combustion timings for all fuels versus O_2 concentration in the intake gas for reference injection strategy (SoI_1 = 342 °CA, SoI_2 = 356 °CA). See Fig. 5 for definitions of parameters.

made while analysing the baseline scenarios, that HVO is more tolerant towards high EGR rates. Interestingly, for oxygen concentrations above 17%, the combustion onset remains majorly insensitive to EGR, and also unaffected by fuel. The differences between fuels are much more evident in an analysis of the $HTHR_1$ period. For O_2 concentration changes above 17%, the delta between SoLTHR and $SoHTHR_1$ is more or less constant for all fuels, with HVO a single °CA shorter than for the two other fuels. Reducing O_2 concentration below 17% results in a dramatic delay of $SoHTHR_1$, but HVO exhibits much lower sensitivity to this. Interestingly, the $SoHTHR_2$ is much less affected by either fuel or EGR ratio.

The conclusion, drawn from the analysis of combustion timing, is that the distance between SoLTHR and $SoHTHR_2$ is almost constant and independent of fuel or EGR. However, the $HTHR_1$ stage is strongly affected by EGR and fuel, both in terms of timing and completeness of combustion. Thus, the local conditions during the combustion of the main fuel are altered.

3.1.3. *Effect of injection strategies on combustion*

These observations made in the previous subsection indicate the need to compensate for the EGR effect with injection timing. Due to the fact that main sensitivities manifest in the combustion stages pertaining to the pilot injection, the effect on combustion of varying SOI_1 is studied in detail in this subsection. The HRRs of selected points from the test protocols shown in Table 4 are presented in Figs. 10 and 11 for the non-EGR and 35% EGR cases, respectively. Additionally, the single-pulse CDC case is presented for reference. Detailed discussion of combustion characteristics is confined to DF and HVO fuels.

Fig. 10 indicates that for the non-EGR conditions, changing the pilot injection timing influences mainly the LTHR and $HTHR_1$ combustion phases. The effect is similar in the case of both DF and HVO. Retarded SoI_1 shifts the combustion onset in these phases towards TDC. At the same time, the $HTHR_1$ combustion phase becomes more rapid with higher peak HRRs. For the earliest pilot injection, however, the combustion in this phase is not complete which contributes to higher peak HRRs in the $HTHR_2$ phase. This phase commences at the same CA for both fuels and for pilot injections at baseline (342 °CA) and at 346 °CA. The main phase combustion is slightly retarded (around 1 °CA) for the earlier SoI_1 at 338 CA, which corresponds to low energy released in the $HTHR_1$ phase.

Consequently, for the single injection case (SoI_S = 354 °CA), the combustion is heavily retarded for DF and exhibits excessive peak HRR. Note that without EGR, the better ignition properties of HVO allow it to

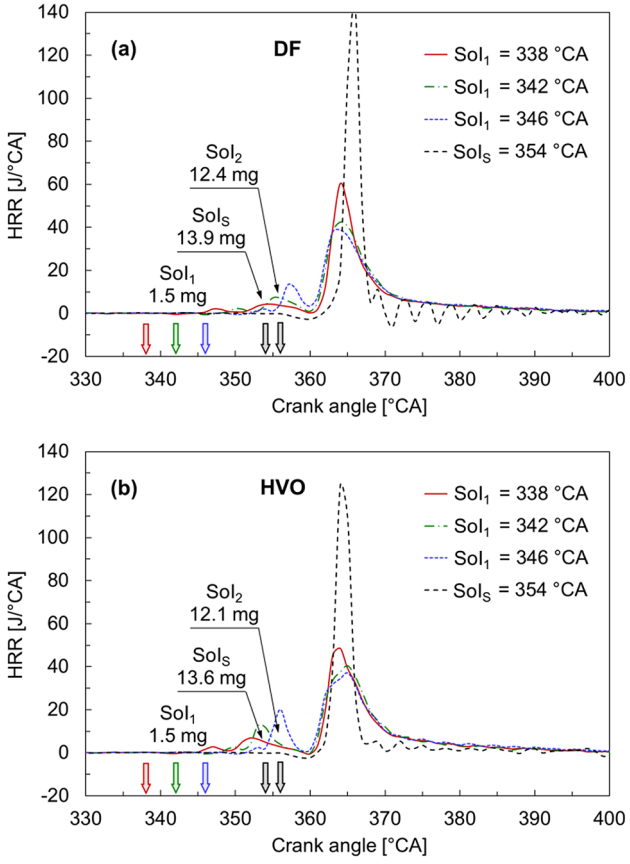

Fig. 10. Heat release rates for all investigated injection strategies for non-EGR operation; a) DF, b) HVO.

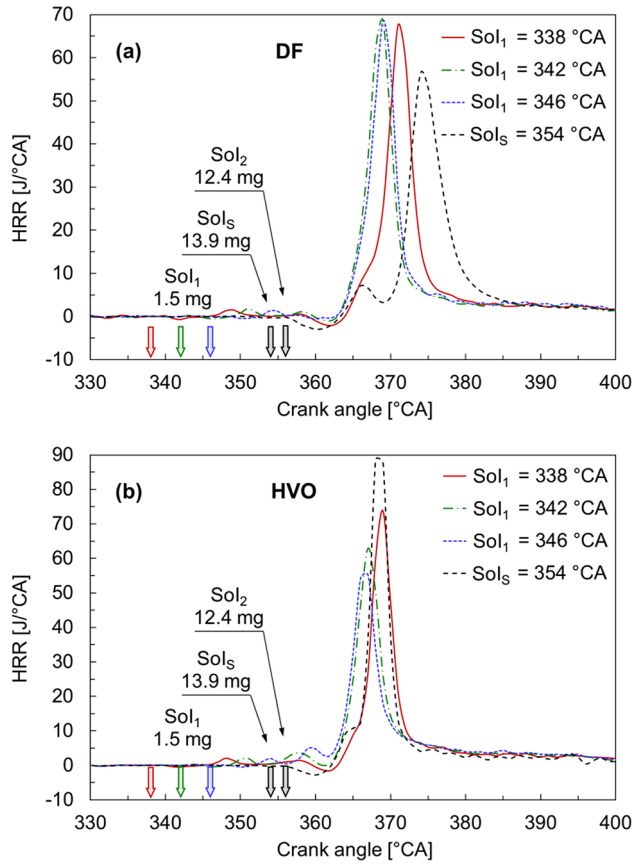

Fig. 11. Heat release rates for all investigated injection strategies for engine operation with 35% EGR (approximately 16% O_2 in the intake gas); a) DF, b) HVO.

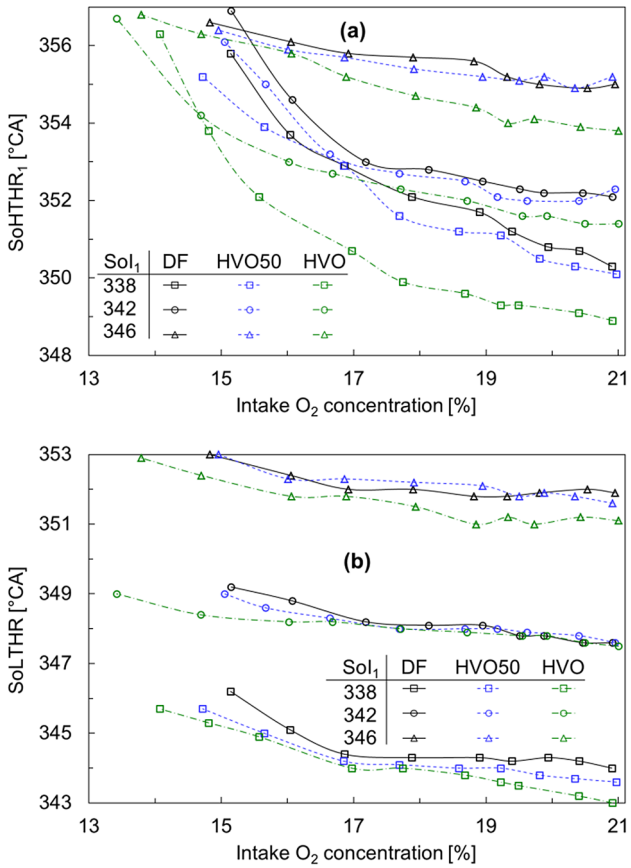

Fig. 12. Start of $HTHR_1$ (a) and start of LTHR (b) versus O_2 concentration in the intake gas for all investigated split fuel-injection schemes. See Fig. 5 for definitions of parameters.

maintain the main SOC close to the baseline case, without the support of hot combustion by-products from the pilot injection. At the same time, the shorter mixing period makes HVO's peak HRR significantly lower than DF's with the same single-pulse strategy.

Introducing EGR results in similar effects as earlier discussed for the baseline injection strategy. Fig. 11a reveals that for DF, the cold flames and the high-temperature reactions associated to the pilot dose are almost negligible, irrespective of the pilot injection timing. Consequently, initiation of the main combustion phase becomes insensitive to changes in this parameter. However, for the early SoI_1, combustion is substantially slower than with the two later cases. This slowdown is associated with the fact that any oxidation attributed to the pilot is finished long before the main injection commences, changing the combustion mechanism from flame propagation (ignition from hot combustion front) towards autoignition with cylinder wall interaction. This effect is magnified for the single-pulse reference, as seen in Fig. 11a. Additionally, clear two-stage (premixed and diffusion) combustion can be noted. HVO in the EGR regime exhibits lower sensitivity in combustion behaviour with respect to injection strategy, as shown in Fig. 11b. Interestingly, it is apparent that the single-pulse reference actually combusts earlier than the early pilot strategy.

Extrapolation of those combustion trends towards higher EGR regimes can be seen in Fig. 12, where the locations of SoLTHR and $SoHTHR_1$ are plotted for different fuels and all split injection strategies. The trends for the baseline SoI_1 at 342 °CA are already discussed in Subsection 3.1.2, so the following observations focus on specific effects when adopting the advanced and retarded injection strategies.

From Fig. 12b one can note that the SoLTHR follows closely the changes in SoI1, giving a constant ignition delay for all fuels when the EGR rate is low. As O_2 concentration is lowered, combustion retards and the differences between fuel samples and injection strategies increase. Generally, HVO is the least affected by EGR. It is also important to note that the effect of EGR on SoLTHR timing is stronger for early pilot injection.

Differences between fuels, both in terms of their tolerance to EGR as well as their response to injection strategies, become evident when $SoHTHR_1$ is considered. Comparing Fig. 12a and 12b one can immediately note that for the latest SoI_1 = 346 °CA, the EGR dependency of $SoHTHR_1$ follows that of SoLTHR. In other words, the angular distance between the two combustion stages is almost constant and the least affected by EGR. In contrast, at SoI_1 = 338 °CA, the response to EGR is far more evident for all fuel samples. At approximately 40% EGR, which reduces oxygen concentration to 15%, $SoHTHR_1$ with all fuels is as much as 5 °CA later than with the non-EGR case. However, $SoHTHR_1$ appears approximately 2 °CA earlier for HVO fuel than for DF. This gives HVO better tolerance to low oxygen conditions, enabling use of higher EGR rates. Interestingly, for all fuels and injection strategies, the boundary of permissible combustion delay is at 357 °CA. Combustion became unstable and highly incomplete beyond this point (see Figs. 16 and 17 for reference).

The general conclusion to be drawn from the above analysis is that the changes of combustion timings for DF and HVO50 are similar, whereas HVO exhibits an earlier high temperature period and lesser vulnerability to EGR. As a result, combustion of pure HVO tolerates higher EGR levels without substantial deterioration of combustion rates.

Fig. 13 shows locations of CA50 for all split injection schemes and all fuels through the range of O_2 concentrations. Although the general trends as EGR rates change are consistent for $SoHTHR_1$ (see Fig. 12a) and CA50, the relationships depend upon the fuel and the injection

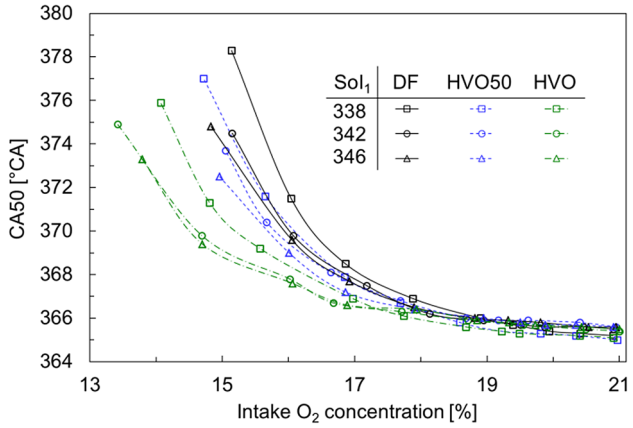

Fig. 13. Location of CA50 versus O_2 concentration in the intake gas for all investigated split fuel-injection schemes.

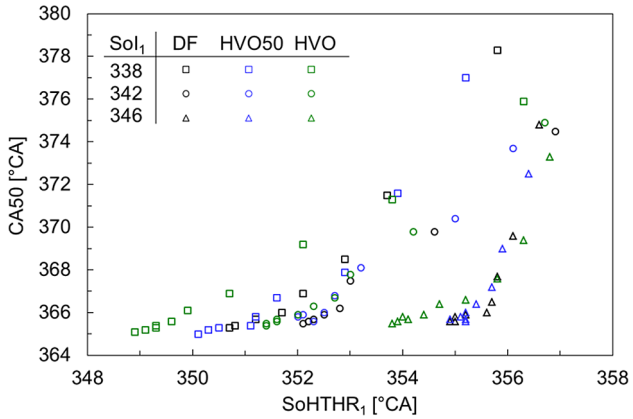

Fig. 14. Correlation between CA50 and $SoHTHR_1$ for all split fuel-injection strategies and variable intake O_2 concentrations. See Fig. 5 for definitions of parameters.

strategy. The correlation of CA50 and $SoHTHR_1$ is shown in Fig. 14. It can be noted that the fuel effect is the greatest for early combustion, i.e. for non-EGR cases. There, for comparable CA50 timings, HVO exhibits earlier $SoHTHR_1$. Fig. 12a shows that, independent of injection strategy, the spread of $SoHTHR_1$ with respect to the intake O_2 concentration is the widest for HVO. This complex relationship can be explained by the fact that CA50 resembles the cumulative effect of the locations of the individual combustion stages and heat release distribution between them. For this particular case, the HVO pilot fuel dose burns completely before $HTHR_2$ period starts. The dwell between $HTHR_1$ and $HTHR_2$ periods results in relatively low reaction rate during the second stage. For DF, $HTHR_2$ runs faster, because fuel spray enters the reacting mixture generated by $HTHR_1$, thus ignites earlier. For late combustion, there is better agreement between $SoHTHR_1$ and CA50 for all fuels. In this case, $HTHR_1$ period is delayed and less complete before SoI_2, which enhances interactions between the two HTHR combustion stages. As a result, CA50 follows $SoHTHR_1$. This effect can be also observed when Figs. 6 and 7 are compared.

3.2. Exhaust emissions

3.2.1. Emissions of regulated compounds

Fig. 15 shows nitrogen oxides emission results as a function of intake oxygen concentration. These are discussed for all investigated fuels and pilot injection angles. EGR's characteristic NO_X–reduction ability is clearly evident in Fig. 15's strong trend. Less oxygen availability limits the nitrogen oxidation, while reduced adiabatic exponent of the

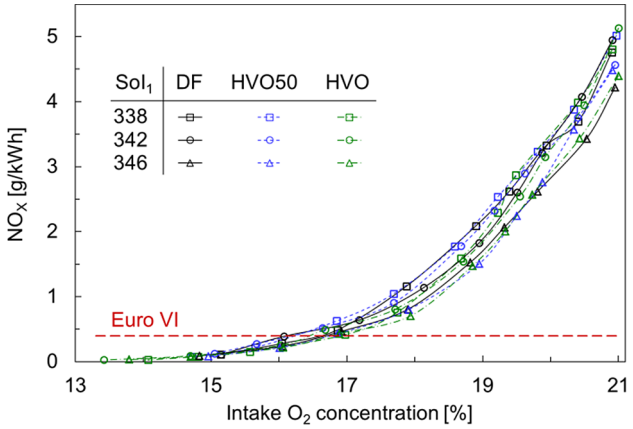

Fig. 15. Indicated specific NO_X emissions versus oxygen concentration in the intake gas for all investigated split fuel-injection schemes.

mixture efficiently suppresses the thermal mechanism of NO_X formation [46].

It is also apparent that with limited EGR, retarding the pilot injection timing can be used to control NO_X to some extent. Interestingly, NO_X emissions seem to be rather insensitive to the type of fuel. However, in the case of HVO, it is notable that at very high EGR rates, although it is penalized by reduced combustion efficiency (see Section 3.2.2), HVO does attain engine-out NO_X levels below 0.4 g/kWh. This paves a way towards meeting the Euro VI emission standard without external exhaust aftertreatment, but this strategy is accompanied by a trade-off related to HC and CO emissions, as discussed below.

A comparison of CO emissions (Fig. 16) with NO_X results (Fig. 15) reveals EGR's typical trade-off behaviour. CO increases exponentially with EGR, which clearly corresponds to higher global and local equivalence ratios. Nevertheless, baseline CO emissions for HVO are below Euro VI's limit of 1.5 g/kWh. As with NO_X, late pilot injections are generally more favourable in terms of reducing CO: for DF and HVO50 this strategy can meet Euro VI's CO limit without EGR. For HVO, SoI adjustment remains neutral towards CO but HVO still exhibits the lowest CO emissions of all the tested samples and across all EGR rates. This is attributed to its lower viscosity.

Total hydrocarbons (THC) emissions are presented in Fig. 17. HVO gives by far the lowest THC emissions, which remain insensitive to a wide range of EGR rates. But even HVO cannot meet Euro VI's THC limit (0.13 g/kWh) without an oxidation catalyst, even using late pilot injections to support more complete combustion. After the EGR rate exceeds 30% (17% O_2), THC emissions escalate due to heavily retarded combustion and flame quenching caused by rapid expansion. The

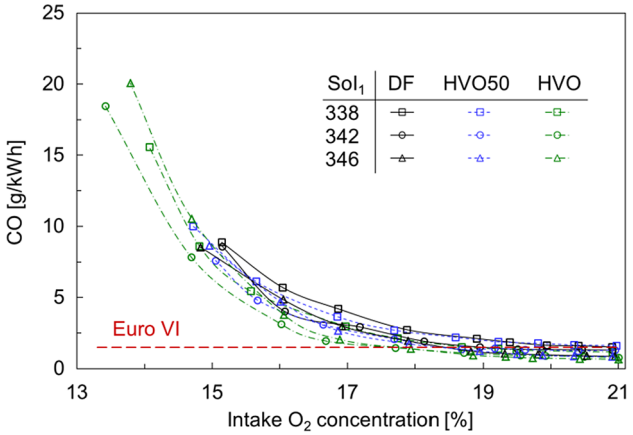

Fig. 16. Indicated specific CO emissions versus oxygen concentration in the intake gas for all investigated split fuel-injection schemes.

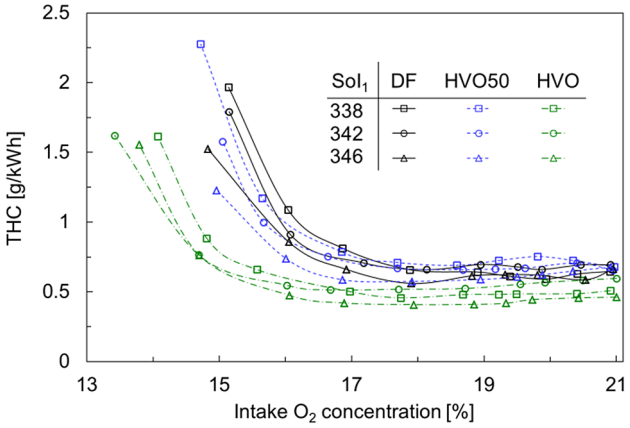

Fig. 17. Indicated specific emissions of total unburned hydrocarbons versus oxygen concentration in the intake gas for all investigated split fuel-injection schemes.

flame-quenching region comes with lower EGR rates for DF and HVO50 because their combustion retardation is greater than with HVO. Note that for all fuels, the point of entry to the flame-quenching region is closely connected to the combustion timing: THC emissions increase when CA50 is delayed. Comparison of Figs. 13 and 17 shows good correlation at higher EGR rates between THC emissions and CA50. This correlation appears to hold good for all the fuels and clearly resembles the effects of different injection strategies.

Although Figs. 15–17 provide interesting insight into the effect of fuel on gaseous emissions, the general trends with EGR are much along the expected lines. But this is not the case for PM emissions, presented in Fig. 18. For both HVO and DF, the trends are non-monotonic and do not conform to the typical NO_X-PM trade-off at heavy EGR conditions. The PM formation mechanism normally is sensitive to O_2 concentration because particulates are formed at regions of local oxygen deficiency. Note, however, that Fig. 18's sharp reduction in PM at diluted mixture conditions is again correlated to excessive retardation of combustion. Long ignition delays allow formation of a largely homogenized mixture, and thus the local combustion temperature drops significantly. The PM thermal creation threshold is around 1700 K for particulates larger than 1 μm (95% of PM created in diesel engines) [47,48]. This is higher than the low-temperature NO_X threshold of the Zeldovich mechanism (around 1370 K) [49] and attainable for low-temperature PPCI strategy. This explains the steep cut-off in PM creation at high EGR rates, observed in Fig. 18.

Fig. 18's differences in the three injection strategies' PM emissions cannot be explained solely by combustion timing, unlike HC emissions.

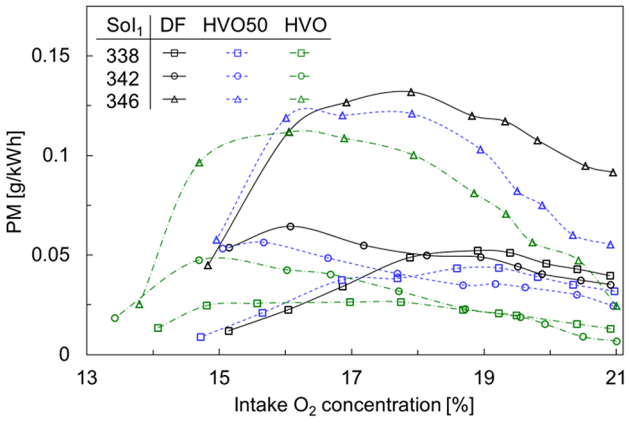

Fig. 18. Indicated specific PM emissions versus oxygen concentration in the intake gas for all investigated split fuel-injection schemes.

Analysis of Fig. 12a, which shows start of individual combustion stages, can contribute to the discussion. Namely, for SoI_1 at 346 °CA, which exhibits by far the largest PM emissions, the $SoHTHR_1$ appears significantly later than for earlier injection strategies. Note, however, that the $SoHTHR_1$ delay (the distance between SoI_1 and $SoHTHR_1$) decreases, favouring diffusion combustion. That translates to higher soot production, while reduces NO_X emissions (refer to Fig. 15), than with the earlier pilot injection cases.

The above reasoning also supports the observed trends in PM emissions, where heavy EGR reduces soot production. PM emissions decrease where EGR provides more significant delay of $SoHTHR_1$. Summarising the trends in Fig. 18, it can be stated that for PM production there is a trade-off between the direct effect of EGR, its resultant local oxygen concentration and combustion delay, which enhances mixing.

Finally, it should be noted that diesel engines equipped with particulate filters usually are calibrated so that PM production is high [50]. Such calibration provides satisfactory NO_X levels while CO and HC emissions are still not increased by falling combustion temperatures. HVO fuel is particularly advantageous in this context, because its CO and HC emissions at high EGR rates are lower than DF's.

3.2.2. *Emissions of selected non-regulated compounds*

The FTIR exhaust analyser used in this study displays concentrations of 23 different species but only aldehydes and aromatics (cumulatively represented by toluene) were selected because they are often reported as being most affected by biofuels [51]. Formaldehyde and acetaldehyde among other carbonyl compounds are most abundant in diesel exhaust. Furthermore, HVO fuels are reported to promote formation of aldehydes but cut-off emissions of aromatics because HVO fuel does not contain them. Finally, both aldehydes and aromatics make a significant contribution to overall exhaust toxicity [14] and so they are of special interest when evaluating replacement fuels.

The trends in formaldehyde (HCHO) emissions, shown in Fig. 19, generally follow those for THC, discussed in Section 3.2.1. However, detailed comparison of Fig. 19 and Fig. 17 reveals that the dynamics of HCHO's increase with the reduction of O_2 concentration is approximately three times higher than that of THC. The ratio of the carbon content in HCHO to THC changes from approximately 0.02 at non-EGR conditions to an average of 0.055 at 15% O_2 concentration. Importantly, with reference to THC, combustion of either pure HVO or HVO50 does not increase HCHO emissions.

The trends in acetaldehyde (CH_3CHO) emissions are shown in Fig. 20. This looks remarkably similar to Fig. 19, demonstrating that production of the two aldehydes is almost the same for all conditions. Finally, it should be underlined that under heavy EGR conditions HVO produces far fewer aldehydes than DF when absolute numbers are

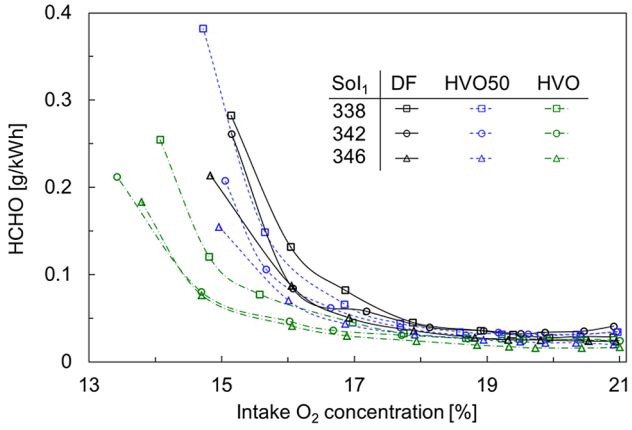

Fig. 19. Indicated specific emissions of formaldehyde versus oxygen concentration in the intake gas for all investigated split fuel-injection schemes.

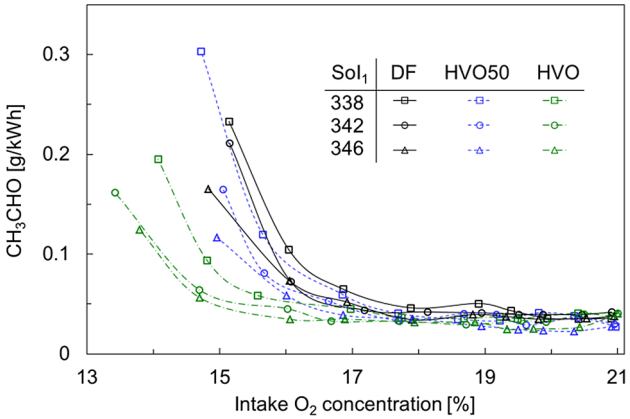

Fig. 20. Indicated specific emissions of acetaldehyde versus oxygen concentration in the intake gas for all investigated split fuel-injection schemes.

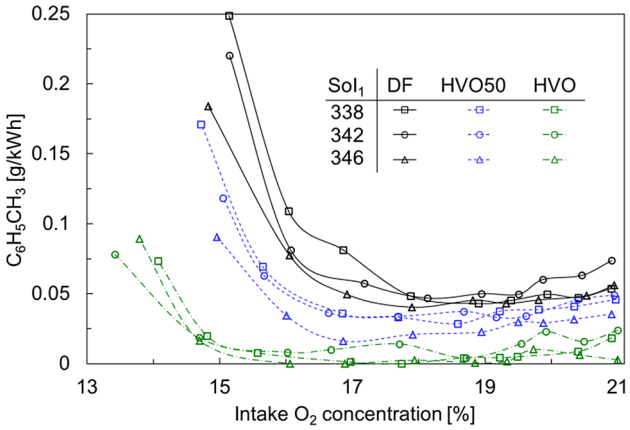

Fig. 21. Indicated specific emissions of aromatic hydrocarbons versus oxygen concentration in the intake gas for all investigated split fuel-injection schemes.

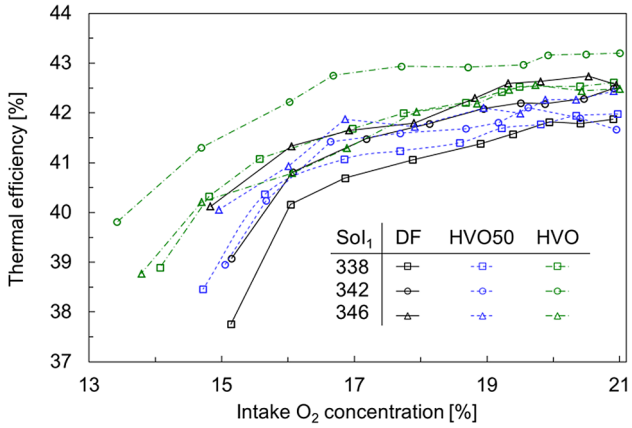

Fig. 22. Indicated thermal efficiency versus oxygen concentration in the intake gas for all investigated split fuel-injection schemes.

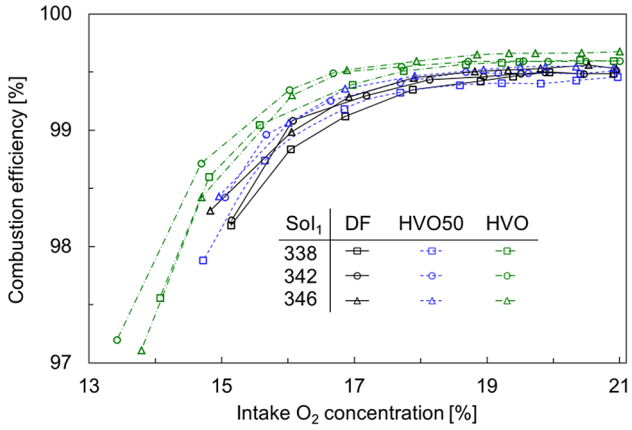

Fig. 23. Combustion efficiency calculated on the basis of CO, THC and soot emissions for all investigated split fuel-injection schemes.

considered. Early pilot injection leads to an increase in emissions of aldehydes when using HVO.

Fig. 21 shows emissions of toluene ($C_6H_5CH_3$), which represents all aromatics in FTIR measurements. As expected, lack of aromatics in biofuel translates to negligible emissions of those compounds, but only for O_2 concentrations above 15%. At the highest applicable EGR rates even pure HVO produced some content of aromatics, constituting 5–6 ppm in terms of molar concentration. Comparing emissions at 15% oxygen concentration, one can note that HVO produces approximately 10 times less aromatics than DF. HVO50's aromatic emissions are larger than the mean value of its two constituent fuels. Pilot injection timing has no effect on HVO's aromatics, but for DF and HVO50 late injection supports reduction of aromatics, just as it does for THC.

3.3. Efficiency analysis

The engine's effectiveness in converting fuel's energy into work is analysed on the basis of indicated thermal efficiency (Fig. 22). Efficiency deteriorating with EGR is a straightforward effect of three factors: (i) retarded combustion onset (ii) lower combustion efficiency (iii) reduced ratio of specific heats. EGR's effect on combustion timing was discussed in detail is Subsection 3.1.3. This study's baseline injection strategy was tuned to achieve optimal location of CA50 for non-EGR conditions. The retardation of CA50 as a consequence of higher EGR rates means the pressure rise is hindered by the expansion, so it is not utilized efficiently for useful work (exhaust losses increase). Furthermore, the accompanying increases of THC and CO emissions at heavy EGR contribute to decreased utilization of fuel's chemical energy and deterioration of combustion efficiency. Fig. 23 shows combustion efficiency, calculated on the basis of unburnt carbon and hydrogen. Combustion losses are generally low for light and medium EGR, at typical levels for PPCI of 0.4–0.6%, increasing significantly for heavy EGR. Note that for all conditions, combustion efficiency is the highest for HVO fuel.

While the above factors (i) and (ii) can be to some extent compensated by the fuel injection strategy, factor (iii) is an inherent consequence of EGR. The following observations about indicated efficiency while operating on different fuels can be drawn from Fig. 22. DF hits the best point indicated efficiency close to 42.6% while operating late pilot injections without or with only minor EGR dilution. At the same operating conditions, addition of HVO to form HVO50 blend led to slightly lower efficiency, but the difference is considered below the level of significance. DF's efficiency showed a clear dependency on pilot SoI timing. Early SoI_1 generally resulted in around 0.9 percentage point lower efficiency than with the late pilot. This dependency diminishes when HVO is admixed to diesel. Finally, for pure HVO, the monotony of the pilot SoI timing trend completely breaks. Now, the baseline injection strategy gives significant improvement, resulting in thermal efficiency of 43.2%. Both earlier and later SoI_1 lowered efficiency, bringing it down to around DF's best point. Although this peculiar effect cannot

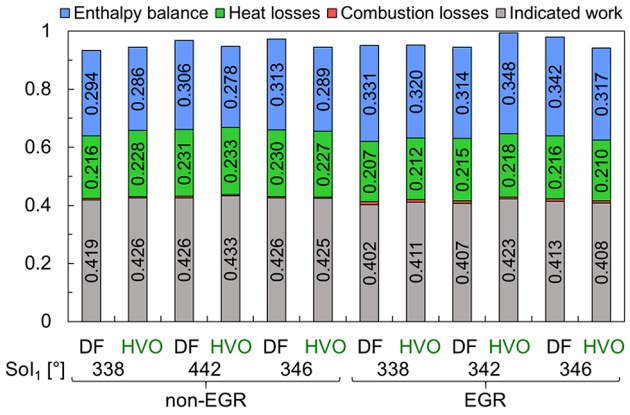

Fig. 24. Energy balance in reference to fuel energy for non-EGR operation and for EGR providing approximately 16% intake O_2. The complement to unity results from uncertainty of the balance.

be explained solely on the basis of CA50 location, Fig. 12a indicates that for other SoI_1 timings, locations of $SoHTHR_1$ are either too early or too late. Additionally, looking at high EGR conditions, HVO's combustion losses are the smallest for the baseline injection strategy.

More insight into differences observed in the fuels' thermal efficiencies is provided by Fig. 24, illustrating the energy breakdown analysis with quantified main losses. The energy balance shows the lower efficiency for EGR cases is indeed mainly through increased exhaust losses, expressed as the enthalpy balance. Although EGR means less exhaust is released from the cylinder than for non-EGR conditions, the higher exhaust temperature and higher specific heats ratio compensate for lower mass flow. Additionally, exhaust temperature, despite the stoichiometry of the mixture, is affected by combustion phasing retard. Note that heat losses are slightly lower for EGR operation, and that DF's heat losses are lower than HVO's by the same order of magnitude. These differences are insufficient to balance the effect of improved combustion phasing and combustion efficiency. The differences in energy balance between different injection strategies are direct effects of heat release distribution between consecutive phases and combustion efficiency.

4. Conclusions

In this work we have investigated the thesis that its better mixing (low viscosity) and its combustion properties (high cetane number) allows HVO and its blends to support attainment of partially premixed compression ignition (PPCI) in a contemporary engine platform. This is evaluated with consideration of efficiency and heavy-duty Euro VI emission legislation, aiming for better trade-off characteristics by co-optimization of injection and EGR strategies.

This high-level thesis is successfully validated, allowing us to formulate a set of conclusions that extend the phenomenological knowledge in the topic:

- The selected baseline injection strategy with 11% of fuel injected as early pilot and the main fuel injected at 356 °CA successfully realizes PPCI combustion. Diffusion flame combustion appears to make a very small contribution, with EGR suppressing the pilot-related heat release in favour of more premixed nature of the main combustion.
- Under such conditions, the combustion characteristics of HVO50, which contains viscosity improvers but has a diesel-like cetane number, are similar to diesel fuel. In contrast, highly reactive HVO exhibits a significantly earlier high temperature period, and accepts high EGR rates (up to 50%) without substantial deterioration of combustion rates and emission indicators.
- The above observation ultimately confirms that the fuel's cetane number dominates its viscosity with regard to achieving highly efficient PPCI combustion.
- The pilot injection timing control can be used to support high EGR dilution without incurring the efficiency/NO_X emission trade-offs that are typical for single-pulse injection, and thus successfully extend the range of efficient PPCI combustion.
- Efficiency deteriorates at ultra-high EGR regimes, as NOx approaches near-zero values and there is rapid increase in THC and CO.
- PM emission has non-monotonic characteristics in PPCI mode, showing a sharp cut-off approaching the PM thermal creation threshold at 40%–45% EGR.

In terms of specific numbers that support applicability of the concept, the following results are worth highlighting:

- On this particular engine platform, at a steady-state, mid-load operating point, HVO allowed 43% indicated thermal efficiency with near-Euro VI engine-out NO_X and CO emissions.
- This result is 1.5 percentage points better than the best, PPCI-optimized, diesel operation.
- At the same time, HVO in PPCI mode proved superior over diesel in terms of CO, PM, and THC emissions, including unlegislated aldehydes and aromatics. The NO_X emissions were on a comparable level.

CRediT authorship contribution statement

Jacek Hunicz: Methodology, Investigation, Writing - original draft, Project administration, Funding acquisition. **Jonas Matijošius:** Resources, Investigation, Funding acquisition. **Alfredas Rimkus:** Resources, Investigation. **Artūras Kilikevičius:** Resources, Investigation. **Paweł Kordos:** Data curation, Visualization. **Maciej Mikulski:** Supervision, Writing - review & editing.

Acknowledgement

The research was financed in the framework of the project Lublin University of Technology, Regional Excellence Initiative, funded by the Polish Ministry of Science and Higher Education (contract No. 030/RID/2018/19). The authors wish to thank AVL List GmbH for making the simulation software available within a framework of the AVL University Partnership Program.

Appendix. Combustion timing data for all investigated conditions

See Table A1.

Table A1
Combustion timing parameters for all investigated conditions.

SOI_1	$SOI_{2/S}$	DF					HVO50					HVO				
		O_2	CA05	CA50	CA95	CA05-95	O_2	CA05	CA50	CA95	CA05-95	O_2	CA05	CA50	CA95	CA05-95
[°CA]	[°CA]	[%]	[°CA]	[°CA]	[°CA]	[°CA]	[%]	[°CA]	[°CA]	[°CA]	[°CA]	[%]	[°CA]	[°CA]	[°CA]	[°CA]
338	356	20.9	356.3	365.2	384.9	28.6	21.0	356.4	365.0	383.7	27.3	20.9	352.9	365.1	383.1	30.2
338	356	20.4	357.2	365.3	385.9	28.7	20.3	356.4	365.2	385.3	28.9	20.4	353.2	365.2	384.8	31.6
338	356	19.9	357.1	365.4	387.3	30.2	19.8	356.9	365.3	385.3	28.4	19.5	353.4	365.3	386.0	32.6
338	356	19.4	358.8	365.7	389.8	31.0	19.2	357.8	365.4	386.8	29.0	19.2	354.1	365.4	386.5	32.4
338	356	18.9	359.6	366.0	390.6	31.0	18.6	359.8	365.8	388.3	28.5	18.7	355.4	365.6	387.8	32.4
338	356	17.9	360.9	366.9	394.1	33.2	17.7	360.8	366.7	388.9	28.1	17.7	357.9	366.1	390.6	32.7
338	356	16.9	364.8	368.5	394.4	29.6	16.9	362.8	367.9	390.4	27.6	17.0	360.2	366.9	392.7	32.5
338	356	16.0	365.9	371.5	395.4	29.5	15.7	366.1	371.6	391.5	25.4	15.6	364.5	369.2	394.2	29.7
338	356	15.1	369.4	378.3	403.5	34.1	14.7	369.3	377.0	392.8	23.5	14.8	366.2	371.3	397.4	31.2
338	356	–	–	–	–	–	–	–	–	–	–	14.1	368.0	375.9	405.3	37.3
342	356	20.9	356.8	365.5	384.1	27.3	21.0	356.1	365.6	384.8	28.7	21.0	353.3	365.4	384.2	30.9
342	356	20.5	356.5	365.6	385.8	29.3	20.4	356.8	365.8	386.6	29.8	20.5	353.5	365.5	385.7	32.2
342	356	19.9	356.6	365.6	386.0	29.4	19.6	357.3	365.9	387.7	30.4	19.9	354.2	365.6	385.5	31.3
342	356	19.5	356.9	365.7	387.3	30.4	19.2	358.1	365.9	388.3	30.2	19.6	354.0	365.7	386.4	32.4
342	356	19.0	357.9	365.9	387.5	29.6	18.7	358.8	366.0	389.4	30.6	18.7	354.7	365.9	388.7	34.0
342	356	18.1	359.9	366.2	389.8	29.9	17.7	361.9	366.8	392.3	30.4	17.7	356.0	366.3	391.6	35.6
342	356	17.2	362.9	367.5	392.2	29.3	16.6	364.0	368.1	393.6	29.6	16.7	357.2	366.7	394.1	36.9
342	356	16.1	365.5	369.8	393.0	27.5	15.7	364.8	370.4	395.1	30.3	16.0	357.9	367.8	395.6	37.7
342	356	15.2	367.4	374.5	395.9	28.5	15.1	368.2	373.7	397.2	29.0	14.7	363.3	369.8	397.8	34.5
342	356	–	–	–	–	–	–	–	–	–	–	13.4	366.7	374.9	400.4	33.7
346	356	21.0	357.2	365.6	390.2	33.0	20.9	356.9	365.6	390.1	33.2	21.0	355.7	365.5	387.5	31.8
346	356	20.5	357.3	365.6	391.0	33.7	20.3	356.9	365.7	390.4	33.5	20.4	355.7	365.6	388.3	32.6
346	356	19.8	357.7	365.8	392.2	34.5	19.9	357.2	365.7	390.4	33.2	19.7	356.0	365.7	388.5	32.5
346	356	19.3	357.9	365.9	393.5	35.6	19.5	357.5	365.8	390.8	33.3	19.3	356.1	365.8	389.6	33.5
346	356	18.8	358.4	366.0	394.6	36.2	19.0	358.3	366.0	392.5	34.2	18.9	356.5	365.9	392.2	35.7
346	356	17.9	361.4	366.5	396.6	35.2	17.9	359.9	366.4	396.4	36.5	17.9	357.6	366.4	395.4	37.8
346	356	16.9	364.0	367.7	397.9	33.9	16.9	362.7	367.2	398.6	35.9	16.9	358.3	366.6	397.6	39.3
346	356	16.1	365.8	369.6	399.6	33.8	16.0	365.6	369.0	399.9	34.3	16.1	361.6	367.6	400.5	38.9
346	356	14.8	368.7	374.8	407.2	38.5	15.0	367.3	372.5	403.6	36.3	14.7	364.8	369.4	402.1	37.3
346	356	–	–	–	–	–	–	–	–	–	–	13.8	367.4	373.3	409.8	42.4
–	354	20.9	364.6	365.6	371.1	6.5	20.9	364.4	365.6	371.2	6.8	21.1	363.3	364.3	371.1	7.8
–	354	20.3	364.9	366.0	371.9	7.0	20.3	364.7	366.0	371.1	6.4	20.3	363.4	364.5	370.8	7.4
–	354	19.8	365.2	366.5	372.6	7.4	19.6	364.8	366.1	371.7	6.9	19.6	363.5	364.7	371.5	8.0
–	354	19.2	365.7	367.2	372.9	7.2	19.1	365.0	366.4	370.7	5.7	19.3	363.3	364.5	371.2	7.9
–	354	19.0	365.9	367.7	373.7	7.8	18.7	365.3	366.9	372.6	7.3	18.9	363.5	364.8	372.6	9.1
–	354	18.0	366.9	369.3	376.5	9.6	17.8	366.1	368.0	374.2	8.0	17.7	364.5	366.2	374.4	9.9
–	354	17.0	368.1	371.7	381.6	13.5	17.0	366.7	369.5	378.0	11.3	16.7	365.0	367.3	378.8	13.8
–	354	16.2	369.5	375.0	391.2	21.7	15.8	368.1	373.0	387.1	19.0	16.1	365.5	368.5	382.9	17.4
–	354	14.8	374.0	391.2	429.7	55.7	14.9	371.2	382.7	409.9	38.7	14.7	366.7	371.6	393.0	26.3
–	354	–	–	–	–	–	–	–	–	–	–	13.7	368.3	377.0	402.1	33.8

References

[1] BP Energy Outlook 2019 edition. Www.bp.com/content/dam/bp/business-sites/en/global/corporate/pdfs/energy-economics/energy-outlook/bp-energy-outlook-2019.pdf. Access 10 Oct. 2019.

[2] Energy demand: Three drivers. ExxonMobil 2019. https://corporate.exxonmobil.com/Energy-and-environment/Looking-forward/Outlook-for-Energy/Energy-demand#transportation . Access 10 Oct. 2019.

[3] Bae C, Kim J. Alternative fuels for internal combustion engines. Proc Combust Inst 2017;36:3389–413. https://doi.org/10.1016/j.proci.2016.09.009.

[4] Aatola H, Larmi M, Sarjovaara T, Mikkonen S. Hydrotreated Vegetable Oil (HVO) as a Renewable Diesel Fuel: Trade-off between NOx, Particulate emission, and fuel consumption of a heavy duty engine. SAE Int J Engines 2008;1:1251–62. https://doi.org/10.4271/2008-01-2500.

[5] Duda K, Wierzbicki S, Śmieja M, Mikulski M. Comparison of performance and emissions of a CRDI diesel engine fuelled with biodiesel of different origin. Fuel 2018;212:202–22. https://doi.org/10.1016/j.fuel.2017.09.112.

[6] Bezergianni S, Dimitriadis A. Comparison between different types of renewable diesel. Renew Sust Energ Rev 2013;21:110–6. https://doi.org/10.1016/j.rser.2012.12.042.

[7] Zöldy M, Török Á. Road transport liquid fuel today and tomorrow: Literature overview. Period Polytech Transp Eng 2015;43:172–6. https://doi.org/10.3311/PPtr. 8095.

[8] Andersson J, Grönkvist S. Large-scale storage of hydrogen. Int J Hydrogen Energy 2019;44:11901–19. https://doi.org/10.1016/j.ijhydene.2019.03.063.

[9] Kivevele TT, Mbarawa MM, Bereczky Á, Zöldy M. Evaluation of the oxidation stability of biodiesel produced from moringa oleifera oil. Energy Fuels 2011;25:5416–21. https://doi.org/10.1021/ef200855b.

[10] Garraín D, Herrera I, Lago C, Lechón Y, Sáez R. Renewable diesel fuel from processing of vegetable oil in hydrotreatment units: theoretical compliance with european directive 2009/28/EC and ongoing projects in spain. Smart Grid Renew Energy 2010;01:70–3. https://doi.org/10.4236/sgre.2010.12011.

[11] Huber GW, O'Connor P, Corma A. Processing biomass in conventional oil refineries: production of high quality diesel by hydrotreating vegetable oils in heavy vacuum oil mixtures. Appl Catal A Gen 2007;329:120–9. https://doi.org/10.1016/j.apcata.2007.07.002.

[12] Šimáček P, Kubička D, Kubičková I, Homola F, Pospíšil M, Chudoba J. Premium quality renewable diesel fuel by hydroprocessing of sunflower oil. Fuel 2011;90:2473–9. https://doi.org/10.1016/j.fuel.2011.03.013.

[13] Vásquez MC, Silva EE, Castillo EF. Hydrotreatment of vegetable oils: A review of the technologies and its developments for jet biofuel production. Biomass Bioenergy 2017;105:197–206. https://doi.org/10.1016/j.biombioe.2017.07.008.

[14] Bünger J, Krahl J, Schröder O, Schmidt L, Westphal GA. Potential hazards associated with combustion of bio-derived versus petroleum-derived diesel fuel. Crit Rev Toxicol 2012;42:732–50. https://doi.org/10.3109/10408444.2012.710194.

[15] Koszalka G, Hunicz J, Niewczas A. A Comparison of performance and emissions of an engine fuelled with diesel and biodiesel. SAE Int J Fuels Lubr 2010;3:77–84. https://doi.org/10.4271/2010-01-1474.

[16] Mollenhauer K, Tschoeke H. Handbook of diesel engines. Springer-Verlag, Berlin Heidelberg 2010. https://doi.org/10.1007/978-3-540-89083-6.

[17] Transport 2013;28(2):158–65. https://doi.org/10.3846/16484142.2013.801364.

[18] Omari A, Pischinger S, Bhardwaj OP, Holderbaum B, Nuottimäki J, Honkanen M. Improving engine efficiency and emission reduction potential of HVO by fuel-

specific engine calibration in modern passenger car diesel applications. SAE Int J Fuels Lubr 2017;10:2017–295. https://doi.org/10.4271/2017-01-2295.
[19] Rimkus A, Žaglinskis J, Stravinskas S, Rapalis P, Matijošius J, Bereczky Á. Research on the combustion, energy and emission parameters of various concentration blends of hydrotreated vegetable oil biofuel and diesel fuel in a compression-ignition engine. Energies 2019;12:2978. https://doi.org/10.3390/en12152978.
[20] Hartikka T, Kuronen M, Kiiski U. Technical performance of HVO (Hydrotreated Vegetable Oil) in diesel engines. SAE Technical Paper 2012–01-1585, 2012.. https://doi.org/10.4271/2012-01-1585.
[21] Bortel I, Vávra J, Takáts M. Effect of HVO fuel mixtures on emissions and performance of a passenger car size diesel engine. Renew Energy 2019;140:680–91. https://doi.org/10.1016/j.renene.2019.03.067.
[22] Vo C, Charoenphonphanich C, Karin P, Susumu S, Hidenori K. Effects of variable O2 concentrations and injection pressures on the combustion and emissions characteristics of the petro-diesel and hydrotreated vegetable oil-based fuels under the simulated diesel engine condition. J Energy Inst 2018;91:1071–84. https://doi.org/10.1016/j.joei.2017.07.002.
[23] Bohl T, Smallbone A, Tian G, Roskilly AP. Particulate number and NOx trade-off comparisons between HVO and mineral diesel in HD applications. Fuel 2018;215:90–101. https://doi.org/10.1016/j.fuel.2017.11.023.
[24] Cheng Q, Tuomo H, Kaario OT, Larmi M. Spray dynamics of HVO and EN590 diesel fuels. Fuel 2019;245:198–211. https://doi.org/10.1016/j.fuel.2019.01.123.
[25] Hulkkonen T, Tilli A, Kaario O, Ranta O, Sarjovaara T, Vuorinen V, et al. Late post-injection of biofuel blends in an optical diesel engine: Experimental and theoretical discussion on the inevitable wall-wetting effects on oil dilution. Int J Eng Res 2017;18:645–56. https://doi.org/10.1177/1468087416663548.
[26] Preuss JK, Munch K, Andersson M, Denbratt I. Comparison of long-chain alcohol blends, HVO and diesel on spray characteristics, ignition and soot formation. SAE Technical Paper 2019–01-0018, 2019.. https://doi.org/10.4271/2019-01-0018.
[27] Millo F, Debnath BK, Vlachos T, Ciaravino C, Postrioti L, Buitoni G. Effects of different biofuels blends on performance and emissions of an automotive diesel engine. Fuel 2015;159:614–27. https://doi.org/10.1016/j.fuel.2015.06.096.
[28] Marasri S, Ewphun P-P, Srichai P, Charoenphonphanich C, Karin P, Tongroon M, et al. Combustion characteristics of hydrotreated vegetable oil-diesel blends under EGR and low temperature combustion conditions. Int J Automot Technol 2019;20:569–78. https://doi.org/10.1007/s12239-019-0054-3.
[29] Agarwal AK, Singh AP, Maurya RK, Shukla PC, Dhar A, Srivastava DK. Combustion characteristics of a common rail direct injection engine using different fuel injection strategies. Int J Therm Sci 2018;134:475–84. https://doi.org/10.1016/j.ijthermalsci.2018.07.001.
[30] Shukla PC, Shamun S, Gren L, Malmborg V, Pagels J, Tuner M. Investigation of Particle Number Emission Characteristics in a Heavy-Duty Compression Ignition Engine Fueled with Hydrotreated Vegetable Oil (HVO). SAE Int J Fuels Lubr 2018;11:495–505. https://doi.org/10.4271/2018-01-0909.
[31] Suarez-Bertoa R, Kousoulidou M, Clairotte M, Giechaskiel B, Nuottimäki J, Sarjovaara T, et al. Impact of HVO blends on modern diesel passenger cars emissions during real world operation. Fuel 2019;235:1427–35. https://doi.org/10.1016/j.fuel.2018.08.031.
[32] Kim D, Kim S, Oh S, No S-Y. Engine performance and emission characteristics of hydrotreated vegetable oil in light duty diesel engines. Fuel 2014;125:36–43. https://doi.org/10.1016/j.fuel.2014.01.089.
[33] Ezzitouni S, Soriano JA, Gómez A, Armas O. Impact of injection strategy and GTL fuels on combustion process and performance under diesel engine start. Fuel 2017;200:529–44. https://doi.org/10.1016/j.fuel.2017.04.012.
[34] Imperato M, Tilli A, Sarjovaara T, Larmi M. Large-bore compression-ignition engines: high NOx reduction achieved at low load with hydro-treated vegetable oil. SAE Int J Fuels Lubr 2012;5:225–32. https://doi.org/10.4271/2011-01-1956.
[35] Lehto K, Elonheimo A, Hakkinen K, Sarjovaara T, Larmi M. Emission reduction using hydrotreated vegetable oil (HVO) with Miller timing and EGR in diesel combustion. SAE Int J Fuels Lubr 2011;5:218–24. https://doi.org/10.4271/2011-01-1955.
[36] Dimitriadis A, Natsios I, Dimaratos A, Katsaounis D, Samaras Z, Bezergianni S, et al. Evaluation of a Hydrotreated Vegetable Oil (HVO) and Effects on Emissions of a Passenger Car Diesel Engine. Front Mech Eng 2018;4:7. https://doi.org/10.3389/fmech.2018.00007.
[37] Lu X, Han D, Huang Z. Fuel design and management for the control of advanced compression-ignition combustion modes. Prog Energy Combust Sci 2011;37:741–83. https://doi.org/10.1016/j.pecs.2011.03.003.
[38] Rohani B, Park SS, Bae C. Effect of injection strategy on low temperature - conventional diesel combustion mode transition. SAE Technical Paper 2015–01-0836, 2015.. https://doi.org/10.4271/2015-01-0836.
[39] Singh AP, Agarwal AK. CI/PCCI combustion mode switching of diesohol fuelled production engine. SAE Technical Paper 2017–01-0738, 2017.. https://doi.org/10.4271/2017-01-0738.
[40] Ewphun P-P, Nagasawa T, Kosaka H, Sato S. Investigation on premixed charge compression ignition combustion control using multi pulse ultrahigh pressure injection. SAE Technical Paper 2019–01-1155, 2019.. https://doi.org/10.4271/2019-01-1155.
[41] Pellegrini L, Beatrice C, Di Blasio G. Investigation of the effect of compression ratio on the combustion behavior and emission performance of HVO blended diesel fuels in a single-cylinder light-duty diesel engine. 2015–01-0898 SAE Technical Paper2015. https://doi.org/10.4271/2015-01-0898.
[42] Neste Renewable Diesel Handbook - Reports 2016. https://docgo.net/viewdoc.html?utm_source=neste-renewable-diesel-handbook. Access 20 Feb. 2019.
[43] Liu H, Tang Q, Yang Z, Ran X, Geng C, Chen B, et al. A comparative study on partially premixed combustion (PPC) and reactivity controlled compression ignition (RCCI) in an optical engine. Proc Combust Inst 2019;37:4759–66. https://doi.org/10.1016/j.proci.2018.06.004.
[44] Srivatsa CV, Mattson J, Depcik C. Performance and emissions analysis of partially pre-mixed charge compression ignition combustion. ASME 2018 Int. Mech. Eng. Congr. Expo., American Society of Mechanical Engineers; 2018, p. V08AT10A018. https://doi.org/10.1115/IMECE2018-86410.
[45] Heywood JBCN-TH. Internal combustion engine fundamentals. Second edi. New York: McGraw-Hill Education; 2018. p. 2018.
[46] Mikulski M, Duda K, Wierzbicki S. Performance and emissions of a CRDI diesel engine fuelled with swine lard methyl esters–diesel mixture. Fuel 2016;164:206–19. https://doi.org/10.1016/j.fuel.2015.09.083.
[47] Merkisz J, Pielecha J. The Process of Formation of Particulate Matter in Combustion Engines. Nanoparticle Emiss. From Combust. Engines, vol. 8, Cham: Springer International Publishing; 2015, p. 19–25. https://doi.org/10.1007/978-3-319-15928-7_3.
[48] Zhang L, Ninomiya Y, Yamashita T. Formation of submicron particulate matter (PM1) during coal combustion and influence of reaction temperature. Fuel 2006;85:1446–57. https://doi.org/10.1016/j.fuel.2006.01.009.
[49] Mikulski M, Bekdemir C. Understanding the role of low reactivity fuel stratification in a dual fuel RCCI engine – A simulation study. Appl Energy 2017;191:689–708. https://doi.org/10.1016/j.apenergy.2017.01.080.
[50] Johnson T, Joshi A. Review of vehicle engine efficiency and emissions. SAE Int J Engines 2018;11:1307–30. https://doi.org/10.4271/2018-01-0329.
[51] Prokopowicz A, Zaciera M, Sobczak A, Bielaczyc P, Woodburn J. The effects of neat biodiesel and biodiesel and HVO blends in diesel fuel on exhaust emissions from a light duty vehicle with a diesel engine. Environ Sci Technol 2015;49:7473–82. https://doi.org/10.1021/acs.est.5b00648.